Transferability of an individual- and trait-based forest dynamics model: A test case across the tropics

E-Ping Rau, Fabian Fischer, Émilie Joetzjer, Isabelle Maréchaux, I Fang Sun, Jérôme Chave

Transferability of an individual- and trait-based forest dynamics model: a test case across the tropics

E-Ping Rau[a], Fabian Fischer[a], Émilie Joetzjer[b], Isabelle Maréchaux[c], I Fang Sun[d], Jérôme Chave[a*]

[a]Laboratoire Évolution et Diversité Biologique (UMR5174) Bâtiment 4R1, 118 route de Narbonne, 31062 Toulouse cedex 9, France

[b] INRAE, Universite de Lorraine, AgroParisTech, UMR Silva, Nancy, France

[c]AMAP Lab, University of Montpellier, INRAE, CIRAD, CNRS, IRD, F-34000 Montpellier, France

[d]Department of Natural Resources and Environmental Studies, National Dong Hwa University, Hualien, Taiwan

[*]Corresponding author

Abstract

Individual-based forest models (IBMs) are useful to investigate the effect of environment on forest structure and dynamics, but they are often restricted to site-specific applications. To build confidence for spatially distributed simulations, model transferability, i.e. the ability of the same model to provide reliable predictions at contrasting sites, has to be thoroughly tested. We tested the transferability of a spatially explicit forest IBM, TROLL, with a trait-based species parameterization and global gridded climate forcing, by applying it to two sites with sharply contrasting climate and floristic compositions across the tropics, one in South America and one in Southeast Asia. We identified which parameters are most influential for model calibration and assessed the model sensitivity to climatic conditions for a given calibration. TROLL produced realistic predictions of forest structure and dynamics at both sites and this necessitates the recalibration of only three parameters, namely photosynthesis efficiency, crown allometry and mortality rate. All three relate to key processes that constrain model transferability and warrant further model development and data acquisition, with mortality being a particular priority of improvement for the current generation of vegetation models. Varying the climatic conditions at both sites demonstrate similar, and expected, model responses: GPP increased with temperature and irradiance, while stem density and aboveground biomass declined as temperature increased. The climate dependence of productivity and biomass was mediated by plant respiration, carbon allocation and mortality, which has implications both on model development and on forecasting of future carbon dynamics. Our detailed examination of forest IBM transferability unveils key processes that need to improve in genericity before reliable large-scale implementations can be envisioned.

Keywords: TROLL, forest simulations, model calibration, climate forcing, Taiwan, Amazonia

1. Introduction

Forests harbor more than half of the total terrestrial biodiversity (Gardner et al., 2010) and contribute to climate change mitigation (Ellison et al., 2017; Mitchard, 2018). However, forest disturbances are important drivers of canopy cover change and they will likely impact tropical forest structure, diversity, and functioning in the future (Feng et al., 2018; Malhi et al., 2009; Zemp et al., 2017). These projections depend on a detailed understanding of the processes that link the abiotic environment and forest dynamics, as can be achieved through integration into simulation models (Fisher et al., 2018; Shugart et al., 2018). Confronting the robustness, reliability and realism of such models is crucial to gain confidence in their predictions (Prentice et al., 2015).

Dynamic global vegetation models (DGVMs) adopt a coarse representation of the coupling between vegetation and biogeochemical cycles. Their simplified description of vegetation dynamics assume a limited set of vegetation structure and summarize plant diversity with a few plant functional types (PFTs). Modern DGVMs simulate demographic processes and trait variability (Fisher et al., 2010; Koven et al., 2020; Sakschewski et al., 2015; Sato et al., 2007; Scheiter et al., 2013). However, difficulties remain in representing plant recruitment and mortality, translating into uncertainties in model projections of forest dynamics (Fisher et al., 2018).

Unlike DGVMs, individual-based forest models (IBMs) explicitly simulate tree establishment, growth, competition, and mortality, simulating forest structure and dynamics at the stand scale (Bugmann, 2001; DeAngelis and Grimm, 2014; Fischer et al., 2016; Shugart, 1984). Forest IBMs adopt a fine-grained representation of the diversity and structure of tree assemblages, which facilitates the exploration of mixed-species forest responses to climate variability (Maréchaux et al., 2021). One drawback is that the calibration of forest IBMs is data demanding, and requires data at a fine spatial and temporal scale. For this reason, IBMs have traditionally been restricted to stand-scale application, and even if their extension to regional or global scale is technically possible (Shugart et al., 2018, 2015), one fundamental challenge is to explore the model validity across space.

At the heart of model upscaling is the question of model transferability (Wenger and Olden, 2012; Yates et al., 2018): when a model has been calibrated at one site, how well does it simulate the vegetation dynamics at another site? Model

transferability hinges upon how well the model is able to capture forest processes at any given site, and on whether the same biogeochemical and biophysical processes hold across sites (Fyllas et al., 2017; Sullivan et al., 2020). For instance, process-based models couple forest processes to environmental drivers in a generic way, through mechanistic modules, such as photosynthesis, water uptake, allocation. These processes are parameterized locally through measurable traits with consistent biological and ecological meaning (e.g. functional traits). This means that, in theory, a completely process-based model should be transferable to any site, provided that measurements of the environmental drivers (e.g., climatic variables) and relevant traits of all locally present tree species are available.

However, for some processes, current knowledge is insufficient to develop generic functions, and a simplified representation is necessary to encapsulate finer processes mediated by environmental, biogeographic or evolutionary factors. As a result, part of the site-specificity is hidden in the model equations and parameters themselves. These site-specific parameters need to be re-calibrated from one site to the other to ensure reliable simulation outputs, which increases calibration efforts and hampers transferability (Lehmann and Huth, 2015; Maréchaux et al., 2021). Even generic equations have typically been formulated using input data from specific sites and under specific conditions, which will not always be consistent with the data provided for model initialization at other sites (Huber et al., 2018). This issue is especially important for tropical forests, which have high variability in composition, structure and functioning within and between sites, making model transferability and upscaling a greater challenge (Castanho et al., 2016; Johnson et al., 2016; Townsend et al., 2008).

Model transferability in part depends on the availability of standardized and spatially distributed data on forest structure and function. For example, site-specific information can be prescribed for a model through trait-based data on floristic diversity (Fyllas et al., 2014, Maréchaux and Chave, 2017) or remote sensing data (Fischer et al., 2019; Joetzjer et al., 2017; Shugart et al., 2015). Consistent climatic boundary conditions, derived from weather models and data assimilation systems, also increase model transferability (Bugmann and Fischlin, 1996; Fauset et al., 2019). This also facilitates the evaluation of how a model responds to changes in climate forcing conditions: for example, in light-limited tropical rainforests, we expect that GPP will exhibit weakly positive or even negative relationship with increasing

121 temperature, due to increasing competition, mortality and faster turnover (Allen et al.,
122 2010; Clark et al., 2010; McDowell et al., 2018).
123 Another way to improve model transferability is to convert modules that are
124 implicitly site-specific into more generic formulations that encode site-specific
125 conditions only through dependence on environmental and floristic composition. This
126 can be facilitated by performing tests to identify model processes that are currently
127 particularly site-specific: the improvement of the representation of those processes,
128 through theoretical and empirical work across multiple sites, should then be
129 prioritized. For instance, we expect that outputs of forest IBMs will be highly
130 sensitive to parameters of mortality, and a more accurate mechanistic representation
131 of mortality should improve the reliability of model projections under conditions
132 beyond the range of the original calibration data (Johnson et al., 2016; Bugmann et
133 al., 2019). Although several studies have explored the issue of transferability of forest
134 IBMs (Bugmann and Solomon, 1995; Lagarrigues et al., 2015; Ma et al., 2017;
135 Shuman et al., 2015), they have so far been limited to temperate and boreal forests
136 with low tree species diversity.
137 In this study, we explored the conditions of transferability of a forest IBM
138 between two contrasting tropical forest sites chosen to maximize dissimilarity in
139 geography, floristic composition and environmental conditions, evaluating separately
140 the effect of parameter calibration and of climate forcing. We asked the following
141 questions:
142 (1) How well does a locally calibrated forest IBM perform when transferred at
143 another site? We expect a degradation of model performance with no fine-tuning at
144 the contrasting site.
145 (2) What key parameters determine model performance during model transfer?
146 We expect that, since most fundamental processes are captured by generic
147 formulations in the model, only few parameters will be identified as in need of
148 recalibration: these parameters point to limitations in model representation of the
149 underlying processes.
150 (3) What are the expected responses to climatic conditions? In the absence of
151 water limitation, as in light-limited rainforests, GPP should increase with temperature
152 and irradiance, while biomass should depend less on temperature.
153

2. Materials and methods

2.1 Model description

The TROLL model is a spatially explicit individual-based model in which the aboveground space of a forest stand is divided into 3D cells of size 1 m^3 (hereafter called voxels; Chave, 1999; Maréchaux and Chave, 2017). Solar irradiance (photosynthetic photon flux density, PPFD) is computed inside each voxel as the irradiance fraction transmitted immediately above the focal voxel. We considered only vertical light transmittance in the canopy; for trees at the edge of the simulated plot, we simulate light interception only for the part of the crown that is inside the plot, and then scale total assimilation with crown radius. At most, one tree can establish in each 1 × 1 m pixel at any given time, and only self-standing stems ≥ 1 cm in trunk diameter at breast height (DBH) are explicitly modelled (herbaceous plants and lianas are not included). The effects of topography and water balance are not modeled. Seeds and seedlings < 1 cm DBH are indirectly modeled as part of a regeneration compartment, with inputs from an external seed rain and seed production within the simulated stand. Each modelled tree is a 3D object, characterized by DBH, height, crown radius, crown depth, total leaf surface area, and age. Trees are assigned species-specific trait values, which influence processes such as photosynthesis, growth and mortality.

At each monthly timestep, the model simulates carbon assimilation (photosynthesis), respiration, carbon allocation and growth for each tree, and also simulates seed dispersal or tree death when conditions are met. Tree growth is the result of an explicit balance between carbon assimilation (photosynthesis) and respiration. Carbon assimilation is represented with the C3 photosynthesis model (Farquhar et al., 1980), which depends on temperature, irradiance, vapor pressure deficit (VPD), and atmospheric CO_2 concentration. During a monthly timestep, photosynthesis is calculated over half-hourly periods of a representative day (monthly mean values of temperature, irradiance and VPD); atmospheric CO_2 concentration is assumed constant. Stomatal conductance is modelled following Medlyn et al. (2011). We define the parameter φ (quantum carbon yield per quantum photon) as the initial slope of the photosynthetic carbon assimilation against irradiance curve; this parameter controls carbon uptake in light-limited conditions (Farquhar et al., 1980). The value of φ depends on environment and species, and it has been shown to be an

187 important source of uncertainty in vegetation models (Domingues et al., 2014;
188 Mercado et al., 2009).
189 After the gross assimilated carbon is calculated from the photosynthesis model,
190 net assimilated carbon is calculated as the gross assimilated carbon minus respiration.
191 Net assimilated carbon is then allocated into biomass in different organs based on
192 parameters of fixed fractions, resulting in tree growth and leaf flush dynamics in the
193 same timestep. The resulting changes in tree height, crown shape and position, and
194 leaf density will then influence the calculation of the light environment and
195 photosynthesis of each tree in the next timestep.
196 The allometric relationship relating tree height and DBH is assumed to be
197 species-specific, while allometric functions relating DBH and crown size are assumed
198 the same for all trees. Crown radius grows as a function of DBH, following a non-
199 linear relationship: $CR = e^{(CR_a + CR_b \times \ln DBH)}$ where CR_a and CR_b are general
200 parameters provided in input. Hence higher CR_a indicates larger crowns for trees of
201 all sizes, whereas higher CR_b indicates that larger trees have disproportionately larger
202 crowns than smaller trees. Identical values of CR_a and CR_b are prescribed for all
203 species given the paucity of available data, even if it is acknowledged that crown size
204 allometry can vary within species, across species and across sites (Jucker et al., 2017;
205 Loubota Panzou et al., 2021).
206 In TROLL, tree mortality results from several processes: (i) stochastic mortality,
207 modelled as function of a maximal background mortality rate m and a linearly
208 decreasing relationship with species-specific wood density (WD), so that: $m_{eff} =$
209 $m - \alpha \times WD$ (α being positive, m is the maximal possible value of the mortality
210 rate); (ii) carbon starvation if net assimilated carbon is negative over a consecutive
211 period exceeding leaf lifespan, so that old leaves have all died while no new leaves
212 could be produced (assuming no internal carbon storage); and (iii) stochastic treefall
213 events, assumed to depend on a tree height threshold, where the parameter vC
214 represents the variability of this threshold. Both m and vC hence summarize complex
215 processes that are not modeled mechanistically.
216 A schematic diagram, which illustrates the structures and processes controlling
217 the individual- and community-level dynamics of a forest in the TROLL model, can
218 be found in Maréchaux and Chave (2017) (Appendix S5, Figure S1). Necessary
219 inputs for a run of TROLL include (i) climate forcing data for the simulated location,

(ii) species-specific parameters of plant traits for the simulated forest, and (iii) species-independent parameters. The source code of TROLL (v2.5) is written in C++ and is available at https://github.com/troll-code/troll. On a computing cluster, each simulation of 200 × 200 m and 500 years uses around 15 min of CPU time.

2.2 Global climate forcing

The TROLL model requires the following climate forcing variables: monthly mean values of daytime and nighttime mean temperature, cumulated rainfall, mean wind speed, and daytime mean irradiance, daytime mean vapor pressure deficit (VPD), and average normalized daily variation of temperature, irradiance and VPD.

We used the CRU-NCEP reanalysis as a standardized climate forcing (version 8; version 7 archived at https://rda.ucar.edu/datasets/ds314.3/) (Viovy, 2018). The CRU-NCEP data set is a global gridded (0.5° × 0.5°) sub-daily (6-hourly) climate product spanning the 1901-2016 period. It provides seven climatic variables: temperature, precipitation, wind, downward longwave and shortwave radiations, air specific humidity, and atmospheric pressure, resulting from the combination of observation-based CRU TS 3.2 data (Harris et al., 2014) and model-based NCEP-NCAR data (Kalnay et al., 1996). We constructed reference monthly mean conditions based on the time range 1980-2016, a period for which the most observations are available, in order to ensure higher accuracy (Kistler et al., 2001), and calculated and extracted climatic variables necessary for TROLL input (Appendix A).

2.3 Study site and species parameterization

We parameterized the TROLL model for Nouragues, French Guiana, South America, and Fushan, Taiwan, Southeast Asia. Aside from the difference in climatic patterns, there is no floristic overlap between Nouragues and Fushan, and tree trait distribution at the two sites differ widely: for example, there is no overlap in the interquartile range of leaf mass per area (LMA; $g.m^{-2}$) values (41.62 - 73.86 at Fushan, and 82.71 - 111.45 at Nouragues) and of wood density ($g.cm^{-3}$) values (0.464 - 0.524 at Fushan, and 0.600 - 0.727 at Nouragues).

The Nouragues Ecological Research Station includes a 12-hectare (400 m × 300 m) plot in a moist lowland tropical forest, part of the Amazonian biome. The Nouragues site experiences two months of dry season per year, with mean annual precipitation around 3000 mm, mean annual temperature around 26°C, and a mean

relative humidity around 99% (Bongers et al., 2001). Since plot establishment in 1994, censuses were completed regularly (2001, 2007, 2012, 2017). All self-standing stems DBH ≥ 10 cm were identified, measured, tagged and mapped. The plot has 622 tree species (Chave et al., 2008; Maréchaux and Chave, 2017).

The Fushan Forest Dynamics Plot (FDP) is a 25-hectare (500 m × 500 m) plot in a moist broadleaf subtropical forest in the northeast of Taiwan (Su et al., 2007), and is a part of ForestGEO (Forest Global Earth Observatory; Anderson-Teixeira et al., 2015; Condit, 1998). The Fushan site is under influence of northeasterly monsoon in winter, and frequent typhoon visits in summer and autumn, with mean annual precipitation around 4200 mm, mean annual temperature around 18°C, and a mean relative humidity around 95%. Plot elevation ranges from 600 m to 733 m (Su et al., 2007). Since plot establishment in 2004, censuses were completed every five years, where all self-standing stems with a DBH ≥ 1 cm were identified, measured, tagged and mapped, with a total of 110 recorded tree species in the plot (Su et al., 2007).

Species-specific parameters of TROLL include leaf mass per area (LMA; $g.m^{-2}$), nitrogen and phosphorus content per mass (N_{mass}, P_{mass} $g.g^{-1}$), wood density ($g.cm^{-3}$), maximum DBH (cm), DBH-height allometric parameters, and regional relative abundance. We implemented all 622 species in the model for the Nouragues site: a complete set of measured trait values were available for 163 species, and for the other species, a combination of species-specific values and genus means or abundance-weighted community means were assigned (Maréchaux and Chave, 2017). For the Fushan site, we implemented 94 species for which a complete set of measured trait values were available: this represents ca. 90% of the trees. The methodology of data collection is detailed in Appendix B.

Climatic data were extracted from the CRU-NCEP dataset at both sites. We also used local climate data, in order to force the model simulations. At Nouragues, semi-hourly meteorological data are available from 2013 to 2019, recorded 400 m away from the plot (4° 05' N, 52° 41' W). At Fushan, daily meteorological data are available from 1991 to 2012, with hourly data from 2013 to 2016, recorded at a meteorological station 3 km east of the forest plot (24° 45′ N, 121° 35′ E). A comparison of the local versus gridded climatic conditions is provided in Appendix C.

For all simulations, we simulated forest regeneration from bare soil for a reference plot area of 4 hectares (200 m × 200 m) for a duration of 500 years (6000

monthly timesteps): based on trial simulation, after 500 years, the forest has reached a steady state.

2.4 Global parameter calibration

In addition to species-specific parameters, TROLL includes a set of 41 species-independent parameters (or 'global' parameters). The majority of these parameters can be measured empirically: initialization (plot size, initial size and leaf densities of trees etc.) and trait variability (intraspecific variation and covariance). Other parameters could vary across sites and they are the primary target of this study.

We first performed a preliminary sensitivity analysis on five parameters tested in a previous study (Maréchaux and Chave, 2017), which revealed that the model had a low sensitivity to the light extinction coefficient (k), and to carbon allocation fractions: f_{wood} and f_{canopy}. We also found that stem density was not adequately estimated at Fushan (Appendix D): we hypothesized that asymmetric light competition and tree mortality may be factors shaping stem density. Thus, we focused on the calibration of five parameters (φ, vC, CR_a, CR_b, m; Table 1) for which it is difficult to obtain precise field estimates. We examined model responses by varying these parameters across a range of values, while using fixed values taken from literature for all other parameters, including k, f_{wood} and f_{canopy}.

For φ, vC and m, we generated uniform prior distributions, bounded within the reported value range. CR_a and CR_b, the slope and intercept of the log-transformed crown radius to DBH relationship are strongly correlated, so we generated correlated standard normal distributions using the Cholesky decomposition assuming a Pearson's r of 0.8, then transformed them to Beta prior distributions (of Beta(2, 2)), bounded within the empirically observed value ranges.

We performed 500 calibration runs for both study sites. For each simulation, three parameters (φ, vC and m) were randomly drawn from the uniform prior distribution, and the two crown allometry parameters (CR_a and CR_b) were drawn as a pair from the correlated Beta prior distributions. Goodness of fit was assessed using four summary metrics: stem density (DBH ≥ 10 cm; N_{10}, trees ha^{-1}), large stem density (DBH ≥ 30 cm; N_{30}, trees ha^{-1}), aboveground biomass (AGB, Mg ha^{-1}), and gross primary productivity (GPP, MgC ha^{-1} yr^{-1}). These metrics summarize both forest structure and functioning and overall constrain the model well. Empirical

values for these metrics were obtained from census data for N_{10}, N_{30} and AGB, and from a global gridded database for GPP (Madani and Parazoo, 2020).

For each summary metric and each simulation, we calculated the steady-state value (defined as the mean over the last 100 years of simulation), and qualitatively described trends of model outcome and model sensitivity to each parameter using scatter plots of parameters against output metrics (Appendix E). Model goodness-of-fit was derived from individual summary statistics using an Euclidean distance between the simulated metrics and empirical values (centered and scaled), and we reported median and interquartile range of parameter values of the simulations with the 10% best overall fit (i.e., 50 best simulations out of 500).

We quantified parameter "informativeness", i.e. the degree to which the dispersion of the posterior parameter distribution is reduced compared to the prior distribution, using the ratio between the interquartile range (IQR) of the best-fit simulations to that of all simulations: a smaller ratio indicates higher parameter informativeness. Finally, we reported the temporal trends of the four summary metrics, and discussed their fit with field observation values.

2.5 Forest response to climatic conditions: a virtual experiment

To study the dependence of forest structure and dynamics on temperature, irradiance and VPD, we performed the following simulated experiment. In the CRU-NCEP dataset, we selected a subset of points corresponding to lowland light-limited rain forest within the 35°N – 35°S latitude range, based on elevation (< 1000 m), climate (annual precipitation > 2000 mm yr^{-1}; Guan et al., 2015; Wagner et al., 2016), and land cover (ESA 'forest' CCI Land Cover classes: 50, 60, 70, 80, and 90). At both study sites, we then performed 500 simulations, each time using the three climatic variables at a randomly sampled point within the selected subset, and using "optimal parameter values", the general parameter values of the one simulation that provided the best overall fit during calibration with the initial climatic condition (Table 2). The aim of this experiment is to explore the response of a forest stand as its climate forcing changes, with a range and correlation structure between the climatic variables that are realistic for tropical forests, and to examine if this climate effect is consistent between sites.

To select the reference pixels, we used precipitation data from CRU-NCEP, the C3S Global Land Cover product for 2018 (accessible at

https://maps.elie.ucl.ac.be/CCI/viewer/download.php; ESA, 2017), and elevation data from the SRTM product (accessible at http://www.earthenv.org/topography) (Amatulli et al., 2018). We used the *gdal_translate* utility to rescale the Land Cover data (300 m × 300 m) and elevation data (1 km × 1 km) to match the spatial scale of CRU-NCEP (0.5° × 0.5°). This resulted in a set of 3753 "reference climate" pixels, of which we randomly sampled 500, using the corresponding climatic variables to force simulations for both Fushan and Nouragues.

To evaluate model sensitivity, we used the same four summary metrics (N_{10}, N_{30}, AGB, GPP). For each metric, we calculated the steady-state value of each simulation (mean value of the last 100 simulated years), and described the trends of model outcome and model sensitivity to each variable using scatter plots of climatic variables against output metrics. In order to quantify the degree of influence of each climatic variable, we fitted linear models with climatic variables as independent terms and the summary metrics as dependent terms, and reported semi-partial coefficients as effect size. Assumptions for linear models were tested and confirmed; two sample points with temperature lower than 15°C were identified as high-leverage points, but their inclusion did not significantly deviate the statistical estimates (Appendix F).

2.6 Data analysis

Data processing, statistical analysis and visualization were performed in R 3.3.0 (R Core Team, 2019). Apart from those already mentioned elsewhere, R packages *ggplot2*, *ggpubr*, *ncdf4*, *raster*, *data.table*, *geosphere*, *sp*, *tidyr*, *extRemes*, and *BIOMASS* were used for this study (Dowle and Srinivasan, 2020; Gilleland and Katz, 2016; Hijmans, 2020, 2019; Kassambara, 2020; Pierce, 2019; Rejou-Mechain et al., 2017; Venables and Ripley, 2002; Wickham, 2020, 2016).

3. Results

Model outcomes were highly sensitive to φ, CR_a and m, and to a lesser extent to CR_b. Higher quantum yield (φ) led to higher large-stem density and AGB and a sharp increase in productivity. Higher overall crown size (larger CR_a values) led to lower stem density and AGB, and a slight increase in productivity; its relationship with large-stem density and AGB was non-linear at Fushan. Higher mortality rates (m) led to reduced large-stem density and AGB (Figure E1 & E2). The parameter values

corresponding to the simulation maximizing the goodness of fit were similar between the two sites for φ and CR_b, but differed markedly for vC, CR_a and m (Table 2).

We used the IQR ratio as measure of parameter informativeness: lower IQR ratio signifies higher informativeness. The most informative parameter was found to be CR_a, informative at both sites (0.55 at Fushan and 0.38 at Nouragues). φ was informative at Nouragues (0.38) but less so at Fushan (0.78), and m was informative at Fushan (0.33) but less so at Nouragues (0.75). CR_b and vC were only moderately informative (values > 0.6 at both sites) (Figure 1).

Temporal change of all four summary statistics (N_{10}, N_{30}, AGB and GPP) were qualitatively similar at both sites, showing sigmoidal increase for stem densities (N_{10} and N_{30}). We observed , a gradual increase of AGB and rapid increase and stabilization of GPP at both sites, and an initial overshoot of N_{10} at Nouragues but not at Fushan (Table 3, Figure 2). At Nouragues, all steady-state estimated metric values showed a good fit to field values; at Fushan, N_{10} was underestimated (ca. 14%), GPP was overestimated (ca. 9%,), and N_{30} and AGB showed reasonably good fit to field values. Both climate forcings yielded similar model outputs, matching well field observations: N_{10} values were similar, N_{30} and AGB values were slightly lower when using ground-based climate forcing at Fushan, and GPP values were markedly lower when using ground-based climate forcing at both sites (Figure 2).

Median climate values across sampled pixels were: temperature = 26.25°C, irradiance = 207.6 $W.m^{-2}$, VPD = 0.644 kPa. Temperature, irradiance and VPD all had significant effects on simulated forest structure and functioning, although effect sizes varied. Temperature effect on N_{10} was strongly negative at Fushan but non-significant at Nouragues; it had strong negative effects on N_{30} and AGB but a weak positive effect on GPP at both sites. Irradiance had a positive effect on all four metrics at both sites, and are especially strong for GPP. VPD had weakly negative effects on GPP at both sites; its effects on the other three metrics were weakly positive at Fushan and non-significant at Nouragues. Overall, effect sizes were weaker at Nouragues than at Fushan (except for irradiance effects on N_{30} and AGB) (Figure 3, Table 4).

4. Discussion

In this study, we tested the transferability of a forest IBM, and demonstrated that the model predicts forest structure and functioning with reasonable accuracy at two

species-rich forest sites in different bioregions. Parameters controlling photosynthetic efficiency, crown allometry and background mortality were found to be key for model calibration. We showed that calibration could help identify influential processes in trait-based forest IBMs and suggests that there is potential of IBM upscaling with improved representation of influential processes and parameter estimation.

4.1 Transferability of an individual-based model

The TROLL model was designed to incorporate a detailed representation of forest diversity while remaining relatively easy to parameterize at a forest site, by prescribing each species using a set of commonly measured traits (Maréchaux and Chave, 2017). This approach alleviates the calibration burden of model transfer (DeAngelis and Grimm, 2014) and facilitates the implementation of large-scale testing of individual-based models. However, not all parameters used in the model are directly observable or easily measurable in the field: some are integrators of multiple processes not explicitly represented within the model. So the issue of model transferability still stands, and we here ask whether a calibrated parameter set for one site performs well elsewhere.

We estimated model parameters through model inversion, comparing model outputs against field observations (Hartig et al., 2012). This approach has been used for several DGVM parameterizations, usually by calibrating against eddy-covariance data (Ichii et al., 2010; Pappas et al., 2013; Restrepo-Coupe et al., 2017). Here, goodness-of-fit depends on four summary statistics of forest structure (stem density) and functioning (biomass and productivity) that are usually available in field inventory data or global gridded data. In the future, the approach could be improved by using the whole height or diameter distribution of the simulated forest, or by adopting a likelihood-based approach (Hartig et al., 2014, 2012).

We calibrated the model at two contrasted tropical forest sites. In spite of their marked differences in climatic conditions, species composition and functional diversity, the simulated forests matched field observations by calibrating a limited subset of parameters. This supports the view that forest models with trait-based parameterization are capable of capturing site-specific characteristics that underpin community dynamics and structure at a given forest site. We speculate that the use of trait-based species parameterization contributes to the reduced need for refitting (i.e., higher model genericity) (Christoffersen et al., 2016; Fisher et al., 2018; Fyllas et al.,

2014; Pappas et al., 2016). Parameters that do differ across sites point to potential improvements in the model, a discussion we now turn to.

4.2 Parameter calibration

We performed calibrations for three parameters that influence predicted forest structure and functioning: photosynthetic efficiency (φ), crown allometry (CR_a), and tree mortality (m). As φ represents the actual quantum yield of photosynthesis (the amount of fixed carbon per light flux absorbed by the chloroplasts), higher φ value results in higher carbon assimilation (when light is limiting) and higher GPP. This parameter only leads to a moderate increase in large stem density (N_{30}) and AGB, and an even smaller effect on overall stem density (N_{10}), indicating that forest demography and biomass accumulation are not solely conditioned by productivity, but also hinge on respiration, carbon allocation, and carbon residence time (Álvarez-Dávila et al., 2017; Johnson et al., 2016; Malhi et al., 2015).

Model calibration was not sensitive to TROLL's species-independent carbon allocation parameters (appendix D), but it should be pointed out that carbon allocation does vary across and even within species (Malhi et al., 2015; Negrón-Juárez et al., 2015). Therefore, including a more mechanistic or trait-mediated representation of carbon allocation may unveil more heterogeneity in forest dynamics, and is an important objective in future model development (Merganičová et al., 2019; Negrón-Juárez et al., 2015; Schippers et al., 2015; Trugman et al., 2019).

In TROLL, crown allometry directly controls light use efficiency and tree competition. Higher CR_a values mean that trees have wider crowns at a given diameter, and achieve higher carbon assimilation rates due to increased light interception, leading to the observed pattern of increase in GPP with increased CR_a. Wider crowns also create more intense shading for smaller trees in the understory and cause higher tree turnover and mortality, leading to the observed pattern of decreasing stem density and AGB. Stand structure also strongly depends on the level of prescribed inter- and intraspecific variability of crown allometry, which determine how complementarity in crown architecture could increase light use efficiency and promote coexistence (Pretzsch, 2019; Vieilledent et al., 2010).

Mortality is an important calibration parameter in TROLL. Tree mortality is a complex process, and in current IBMs, it is often modeled empirically, and thus remains one of the main sources of model uncertainty (Bugmann et al., 2019). In the

FORMIND model, the mortality rate is empirically correlated with environmental variables such as precipitation and soil property, which vary across space (Rödig et al., 2018, 2017). Such simplifications limit our ability to explore how different causes of tree mortality impact forest structure (McDowell et al., 2018).

Natural disturbance events such as fire, drought or wind are responsible for a significant proportion of tree mortality (Fischer et al., 2018; McDowell et al., 2018; Peterson et al., 2019), and they impact forest structure and functioning (Ibanez et al., 2019; Magnabosco Marra et al., 2018; Pugh et al., 2019). The two forest sites selected for this study depend on different wind disturbance regimes: notably, Fushan is influenced by frequent tropical cyclones (Dowdy et al., 2012; Lin et al., 2011), while Nouragues is not exposed to cyclones. At Nouragues, TROLL simulates an overshoot of stem density during early succession, indicating self-thinning, but not at Fushan. One hypothesis for this pattern is that cyclones shape a more open canopy at Fushan, resulting in a less intense self-thinning. This may also explain why the optimal value for the mortality rate (m) is lower at Fushan than at Nouragues. It would be important to devise more mechanistic representations of disturbance events in TROLL.

4.3 Upscaling of individual-based models

Various efforts have been made to upscale IBMs to the regional or global scale. Individual-based approaches have been coupled to or developed within DGVMs (Fisher et al., 2018; Sakschewski et al., 2015; Sato et al., 2007) to represent cohort processes. Ma et al. (2017) prescribed environmental data for simulations of the FORCCHIN IBM model at several flux tower sites, and validated the simulated carbon flux against flux tower data. Rödig et al. (2018, 2017a) performed regionalization for the FORMIND model by calibrating the mortality parameter at a number of sites and correlating it with environmental variables (precipitation and soil properties), and performing simulations at sites over the entire Amazon using mortality parameters predicted from the environmental variables. Simulated temporal dynamics of canopy height were then compared with remote sensing data to determine the succession status of each site, which was then used to generate Amazon-wide estimation of other forest attributes such as biomass and productivity.

Yet, these studies assigned trees to a small number of plant functional types that relied on empirical parameterization. Our study, although smaller in scope, is a proof of concept demonstrating that trait-based IBM upscaling is achievable with minimal

calibration and is therefore realistic in the tropics, provided that trait measurements exist and tree floristic composition is available at the focal site. Moreover, since model output contains detailed information about forest composition, TROLL could also help answer how plant diversity responds to environmental changes.

With every forest model, assumptions are made about which parameters are species-dependent and which are not. The model described here, TROLL, is designed with the aim to contain as much species-specific information that is currently available. For an individual-based model, this choice does not necessarily incur higher computational burden than the plant functional type approach, since in both cases every individual tree is simulated. However, supplying models with species-specific information requires considerably more parameterization effort. With the ongoing collection effort of plant traits in permanent plots around the world, the assembly of global trait databases (Anderson-Teixeira et al., 2015; Chave et al., 2009; Kattge et al., 2020) and development of techniques to measure new plant traits, we expect that it will be easier to generalize this approach to many sites. Here we show that of the species-independent parameters, only a few require site-specific calibration for realistic model output to be achieved, and identifying these parameters helps identifying priorities for future theoretical and modeling development, as well as for field measurements (Medlyn et al., 2016).

4.4 Climate impact on forests using IBMs

Another important part of assessing transferability of forest IBMs consists in evaluating how the model responds to environmental forcing, an important step in understanding how forests respond to climate change (Shugart et al., 2018). We here examined the effect of climate forcing without the need of re-calibration (Fauset et al., 2019; Shugart et al., 2018). Many forest IBMs prescribe climatic conditions based on locally measured data (Ma et al., 2017; Shuman et al., 2015), yet it is important to provide a consistent climate forcing condition even at places where local measurements do not exist, and to ensure comparability among sites. The integration of the gridded CRU-NCEP climate dataset as model input fulfills this condition, and thus further simplifies large-scale implementation.

TROLL simulations at the Fushan and Nouragues sites with different climatic conditions demonstrate that the model reproduces a general pattern of climatic response that remain nearly identical upon model transfer, with only quantitative

differences between sites. The simulated positive relationship of GPP with temperature and irradiance and the negative relationship with VPD are in agreement with expectations (Malhi et al., 2015; Reyer, 2015).Under the current model version, VPD constrains leaf stomatal conductance in the photosynthesis process, and we found a weak effect of VPD. As water availability is one of the key climatic factors that shape forest dynamics and functioning (Álvarez-Dávila et al., 2017; Feng et al., 2018; Galbraith et al., 2010; Poorter et al., 2017), further investigation of forest response to drought and soil water stress is necessary, and will be the focus of future model development.

At both sites, we observed a decoupling between the response of productivity and that of stem density and AGB. With increasing temperature, GPP increased while large tree density and AGB decreased. These observations are consistent with empirical studies that showed that productivity is a poor predictor of biomass in old-growth tropical forests (Johnson et al., 2016; Malhi et al., 2015). Biomass accumulation is controlled by numerous processes other than carbon assimilation, including mortality, functional composition, and size structure (Allen et al., 2010; Bugmann et al., 2019; Johnson et al., 2016).

The Fushan site responded more to variation in climatic conditions than Nouragues. One interpretation of this finding is that the native bioclimatic conditions of Nouragues were closer to the average condition of reference climatic conditions, whereas Fushan has a fringe climatic condition (subtropical). Consequently, constraining the Fushan forest to average tropical forest climatic conditions had more effect than on the Nouragues forest.

4.5 Conclusion and perspectives

We have demonstrated that a detailed exploration of the calibration and transferability of trait-based forest IBMs offers an opportunity to assess the genericity of model assumptions. Even though our results are based on model simulations, they do pave the way towards a much more systematic exploration of model behavior across a wide range of sites that are representative of a variety of forest types.

We here identify two main priorities for future individual-based model development: 1) including more detailed and mechanistic representation of important physiological processes, such as disturbance-driven tree mortality (Seidl et al., 2014, 2011; Uriarte et al., 2009), and 2) improving constraints of key parameters with

detailed and spatially distributed data, such as informing crown allometry with remote sensing data (Calders et al., 2018; Fischer et al., 2020; Shugart et al., 2015). With the help of improvements in these two directions, we argue that upscaling of individual-based vegetation models with detailed, trait-based species description need not be associated with high calibration burden, and that they have great potential for large-scale implementation.

Acknowledgements

Simulations were run on the OLYMPE cluster at CALMIP, Toulouse. We thank Dr. Shiang-Yue Lu and Hui-Hsueh Huang at TFRI (Taiwan Forestry Research Institute) for providing us with the local climate data at the meteorological station were provided by via communications with, whom we thank. This work was supported by the "Investissement d'Avenir" grants managed by the Agence Nationale de la Recherche (CEBA, ref. ANR-10-LABX-25-01; TULIP, ref. ANR-10-LABX-0041; ANAEE-France: ANR-11-INBS-0001).

References

Allen, C.D., Macalady, A.K., Chenchouni, H., Bachelet, D., McDowell, N., Vennetier, M., Kitzberger, T., Rigling, A., Breshears, D.D., Hogg, E.H. (Ted., Gonzalez, P., Fensham, R., Zhang, Z., Castro, J., Demidova, N., Lim, J.H., Allard, G., Running, S.W., Semerci, A., Cobb, N., 2010. A global overview of drought and heat-induced tree mortality reveals emerging climate change risks for forests. For. Ecol. Manage. 259, 660–684. https://doi.org/10.1016/j.foreco.2009.09.001

Álvarez-Dávila, E., Cayuela, L., González-Caro, S., Aldana, A.M., Stevenson, P.R., Phillips, O., Cogollo, Á., Peñuela, M.C., Von Hildebrand, P., Jiménez, E., Melo, O., Londoño-Vega, A.C., Mendoza, I., Velásquez, O., Fernández, F., Serna, M., Velázquez-Rua, C., Benítez, D., Rey-Benayas, J.M., 2017. Forest biomass density across large climate gradients in northern South America is related to water availability but not with temperature. PLoS One 12, 1–16. https://doi.org/10.1371/journal.pone.0171072

Amatulli, G., Domisch, S., Tuanmu, M.N., Parmentier, B., Ranipeta, A., Malczyk, J., Jetz, W., 2018. Data Descriptor: A suite of global, cross-scale topographic variables for environmental and biodiversity modeling. Sci. Data 5, 1–15. https://doi.org/10.1038/sdata.2018.40

Anderson-Teixeira, K.J., Davies, S.J., Bennett, A.C., Gonzalez-Akre, E.B., Muller-Landau, H.C., Joseph Wright, S., Abu Salim, K., Almeyda Zambrano, A.M., Alonso, A., Baltzer, J.L., Basset, Y., Bourg, N.A., Broadbent, E.N., Brockelman, W.Y., Bunyavejchewin, S., Burslem, D.F.R.P., Butt, N., Cao, M., Cardenas, D., Chuyong, G.B., Clay, K., Cordell, S., Dattaraja, H.S., Deng, X., Detto, M., Du, X., Duque, A., Erikson, D.L., Ewango, C.E.N., Fischer, G.A., Fletcher, C., Foster, R.B., Giardina, C.P., Gilbert, G.S., Gunatilleke, N., Gunatilleke, S., Hao, Z., Hargrove, W.W., Hart, T.B., Hau, B.C.H., He, F., Hoffman, F.M., Howe, R.W., Hubbell, S.P., Inman-Narahari, F.M., Jansen, P.A., Jiang, M., Johnson, D.J., Kanzaki, M., Kassim, A.R., Kenfack, D., Kibet, S.,

629 Kinnaird, M.F., Korte, L., Kral, K., Kumar, J., Larson, A.J., Li, Y., Li, X., Liu, S., Lum, S.K.Y.,
630 Lutz, J.A., Ma, K., Maddalena, D.M., Makana, J.-R., Malhi, Y., Marthews, T., Mat Serudin, R.,
631 Mcmahon, S.M., McShea, W.J., Memiaghe, H.R., Mi, X., Mizuno, T., Morecroft, M., Myers,
632 J.A., Novotny, V., de Oliveira, A.A., Ong, P.S., Orwig, D.A., Ostertag, R., den Ouden, J., Parker,
633 G.G., Phillips, R.P., Sack, L., Sainge, M.N., Sang, W., Sri-ngernyuang, K., Sukumar, R., Sun, I.-
634 F., Sungpalee, W., Suresh, H.S., Tan, S., Thomas, S.C., Thomas, D.W., Thompson, J., Turner,
635 B.L., Uriarte, M., Valencia, R., Vallejo, M.I., Vicentini, A., Vrška, T., Wang, Xihua, Wang,
636 Xugao, Weiblen, G.D., Wolf, A., Xu, H., Yap, S., Zimmerman, J.K., 2015. CTFS-ForestGEO: A
637 worldwide network monitoring forests in an era of global change. Glob. Chang. Biol. 21, 528–
638 549. https://doi.org/10.1111/gcb.12712

639 Bongers, F., Charles-Dominique, P., Forget, P.-M., Théry, M., 2001. Nouragues: dynamics and plant-
640 animal interactions in a neotropical rainforest.

641 Botkin, D.B., Janak, J.F., Wallis, J.R., 1972. Some Ecological Consequences of a Computer Model of
642 Forest Growth. J. Ecol. 60, 849–872.

643 Buck, A.L., 1981. New equations for computing vapour pressure and enhancement factor. J. Appl.
644 Meteorol. https://doi.org/10.1175/1520-0450(1981)0202.0.CO;2

645 Bugmann, H., 2001. A Review of forest gap models. Clim. Change 51, 259–305.
646 https://doi.org/10.1017/S0022112088002617

647 Bugmann, H., Fischlin, A., 1996. Simulating forest dynamics in a complex topography using gridded
648 climatic data. Clim. Change 34, 201–211. https://doi.org/10.1007/BF00224631

649 Bugmann, H., Seidl, R., Hartig, F., Bohn, F., Brůna, J., Cailleret, M., François, L., Heinke, J., Henrot,
650 A.J., Hickler, T., Hülsmann, L., Huth, A., Jacquemin, I., Kollas, C., Lasch-Born, P., Lexer, M.J.,

651 Merganič, J., Merganičová, K., Mette, T., Miranda, B.R., Nadal-Sala, D., Rammer, W., Rammig,
652 A., Reineking, B., Roedig, E., Sabaté, S., Steinkamp, J., Suckow, F., Vacchiano, G., Wild, J., Xu,
653 C., Reyer, C.P.O., 2019. Tree mortality submodels drive simulated long-term forest dynamics:
654 assessing 15 models from the stand to global scale. Ecosphere 10.
655 https://doi.org/10.1002/ecs2.2616

656 Bugmann, H.K.M., Solomon, A.M., 1995. The use of a European forest model in North America: a
657 study of ecosystem response to climate gradients. J. Biogeogr. 22, 477–484.
658 https://doi.org/10.2307/2845944

659 Calders, K., Origo, N., Burt, A., Disney, M., Nightingale, J., Raumonen, P., Åkerblom, M., Malhi, Y.,
660 Lewis, P., 2018. Realistic forest stand reconstruction from terrestrial LiDAR for radiative transfer
661 modelling. Remote Sens. 10, 1–15. https://doi.org/10.3390/rs10060933

662 Castanho, A.D.A., Galbraith, D., Zhang, K., Coe, M.T., Costa, M.H., Moorcroft, P., 2016. Changing
663 Amazon biomass and the role of atmospheric CO2 concentration, climate, and land use. Global
664 Biogeochem. Cycles 30, 18–39. https://doi.org/10.1002/2015GB005135

665 Chave, J., 1999. Study of structural, successional and spatial patterns in tropical rain forests using
666 TROLL, a spatially explicit forest model. Ecol. Modell. 124, 233–254.
667 https://doi.org/10.1016/S0304-3800(99)00171-4

668 Chave, J., Coomes, D.A., Jansen, S., Lewis, S.L., Swenson, N.G., Zanne, A.E., 2009. Towards a
669 worldwide wood economics spectrum. Ecol. Lett. 12, 351–366. https://doi.org/10.1111/j.1461-
670 0248.2009.01285.x

671 Chave, J., Olivier, J., Bongers, F., Chatelet, P., Forget, P.-M., van der Meer, P., Norden, N., Riera, B.,
672 Charles-Dominique, P., 2008. Above-ground biomass and productivity in a rain forest of eastern

South America. J. Trop. Ecol. 24, 355–366. https://doi.org/10.1017/S0266467408005075

Christoffersen, B.O., Gloor, M., Fauset, S., Fyllas, N.M., Galbraith, D.R., Baker, T.R., Kruijt, B., Rowland, L., Fisher, R.A., Binks, O.J., Sevanto, S., Xu, C., Jansen, S., Choat, B., Mencuccini, M., McDowell, N.G., Meir, P., 2016. Linking hydraulic traits to tropical forest function in a size-structured and trait-driven model (TFS v.1-Hydro). Geosci. Model Dev. 9, 4227–4255. https://doi.org/10.5194/gmd-9-4227-2016

Clark, D.B., Clark, D.A., Oberbauer, S.F., 2010. Annual wood production in a tropical rain forest in NE Costa Rica linked to climatic variation but not to increasing CO2. Glob. Chang. Biol. 16, 747–759. https://doi.org/10.1111/j.1365-2486.2009.02004.x

Condit, R., 2008. Methods for estimating aboveground biomass of forest and replacement vegetation in the tropics. Cent. Trop. For. Sci. Res. Man.

Condit, R.S., 1998. Tropical forest census plots. Springer Science & Business Media, Berlin/Heidelberg. https://doi.org/10.1007/978-3-662-03664-8

DeAngelis, D.L., Grimm, V., 2014. Individual-based models in ecology after four decades. F1000Prime Rep. 6. https://doi.org/10.12703/p6-39

Domingues, T.F., Martinelli, L.A., Ehleringer, J.R., 2014. Seasonal patterns of leaf-level photosynthetic gas exchange in an eastern Amazonian rain forest. Plant Ecol. Divers. 7, 189–203. https://doi.org/10.1080/17550874.2012.748849

Dowdy, A.J., Qi, L., Jones, D., Ramsay, H., Fawcett, R., Kuleshov, Y., 2012. Tropical cyclone climatology of the South Pacific Ocean and its relationship to El Niño-Southern oscillation. J. Clim. 25, 6108–6122. https://doi.org/10.1175/JCLI-D-11-00647.1

Dowle, M., Srinivasan, A., 2020. data.table: Extension of `data.frame`.

695 Ellison, D., Morris, C.E., Locatelli, B., Sheil, D., Cohen, J., Murdiyarso, D., Gutierrez, V., Noordwijk,
696 M. van, Creed, I.F., Pokorny, J., Gaveau, D., Spracklen, D. V., Tobella, A.B., Ilstedt, U.,
697 Teuling, A.J., Gebrehiwot, S.G., Sands, D.C., Muys, B., Verbist, B., Springgay, E., Sugandi, Y.,
698 Sullivan, C.A., 2017. Trees, forests and water: Cool insights for a hot world. Glob. Environ.
699 Chang. 43, 51–61. https://doi.org/10.1016/j.gloenvcha.2017.01.002

700 ESA, 2017. Land Cover CCI Product User Guide Version 2. Tech. Rep.

701 Farquhar, G.D., von Caemmerer, S., Berry, J.A., 1980. A biochemical model of photosynthetic
702 CO<Subscript>2</Subscript> assimilation in leaves of C<Subscript>3</Subscript> species.
703 Planta 149, 78–90.

704 Fauset, S., Gloor, M., Fyllas, N.M., Phillips, O.L., Asner, G.P., Baker, T.R., Patrick Bentley, L.,
705 Brienen, R.J.W., Christoffersen, B.O., del Aguila-Pasquel, J., Doughty, C.E., Feldpausch, T.R.,
706 Galbraith, D.R., Goodman, R.C., Girardin, C.A.J., Honorio Coronado, E.N., Monteagudo, A.,
707 Salinas, N., Shenkin, A., Silva-Espejo, J.E., van der Heijden, G., Vasquez, R., Alvarez-Davila,
708 E., Arroyo, L., Barroso, J.G., Brown, F., Castro, W., Cornejo Valverde, F., Davila Cardozo, N.,
709 Di Fiore, A., Erwin, T., Huamantupa-Chuquimaco, I., Núñez Vargas, P., Neill, D., Pallqui
710 Camacho, N., Gutierrez, A.P., Peacock, J., Pitman, N., Prieto, A., Restrepo, Z., Rudas, A.,
711 Quesada, C.A., Silveira, M., Stropp, J., Terborgh, J., Vieira, S.A., Malhi, Y., 2019. Individual-
712 Based Modeling of Amazon Forests Suggests That Climate Controls Productivity While Traits
713 Control Demography. Front. Earth Sci. 7. https://doi.org/10.3389/feart.2019.00083

714 Feng, X., Uriarte, M., González, G., Reed, S., Thompson, J., Zimmerman, J.K., Murphy, L., 2018.
715 Improving predictions of tropical forest response to climate change through integration of field
716 studies and ecosystem modeling. Glob. Chang. Biol. 24, e213–e232.

https://doi.org/10.1111/gcb.13863

Fischer, F.J., Labrière, N., Vincent, G., Hérault, B., Alonso, A., Memiaghe, H., Bissiengou, P., Kenfack, D., Saatchi, S., Chave, J., 2020. A simulation method to infer tree allometry and forest structure from airborne laser scanning and forest inventories. Remote Sens. Environ. 251, 112056. https://doi.org/10.1016/j.rse.2020.112056

Fischer, F.J., Maréchaux, I., Chave, J., 2019. Improving plant allometry by fusing forest models and remote sensing. New Phytol. 223, 1159–1165. https://doi.org/10.1111/nph.15810

Fischer, R., Bohn, F., Dantas de Paula, M., Dislich, C., Groeneveld, J., Gutiérrez, A.G., Kazmierczak, M., Knapp, N., Lehmann, S., Paulick, S., Pütz, S., Rödig, E., Taubert, F., Köhler, P., Huth, A., 2016. Lessons learned from applying a forest gap model to understand ecosystem and carbon dynamics of complex tropical forests. Ecol. Modell. 326, 124–133. https://doi.org/10.1016/j.ecolmodel.2015.11.018

Fischer, R., Rödig, E., Huth, A., 2018. Consequences of a reduced number of plant functional types for the simulation of forest productivity. Forests 9. https://doi.org/10.3390/f9080460

Fisher, R.A., Koven, C.D., Anderegg, W.R.L., Christoffersen, B.O., Dietze, M.C., Farrior, C.E., Holm, J.A., Hurtt, G.C., Knox, R.G., Lawrence, P.J., Lichstein, J.W., Longo, M., Matheny, A.M., Medvigy, D., Muller-Landau, H.C., Powell, T.L., Serbin, S.P., Sato, H., Shuman, J.K., Smith, B., Trugman, A.T., Viskari, T., Verbeeck, H., Weng, E., Xu, C., Xu, X., Zhang, T., Moorcroft, P.R., 2018. Vegetation demographics in Earth System Models: A review of progress and priorities. Glob. Chang. Biol. 24, 35–54. https://doi.org/10.1111/gcb.13910

Fyllas, N.M., Bentley, L.P., Shenkin, A., Asner, G.P., Atkin, O.K., Díaz, S., Enquist, B.J., Farfan-Rios, W., Gloor, E., Guerrieri, R., Huasco, W.H., Ishida, Y., Martin, R.E., Meir, P., Phillips, O.,

739 Salinas, N., Silman, M., Weerasinghe, L.K., Zaragoza-Castells, J., Malhi, Y., 2017. Solar
740 radiation and functional traits explain the decline of forest primary productivity along a tropical
741 elevation gradient. Ecol. Lett. 20, 730–740. https://doi.org/10.1111/ele.12771

742 Fyllas, N.M., Gloor, E., Mercado, L.M., Sitch, S., Quesada, C.A., Domingues, T.F., Galbraith, D.R.,
743 Torre-Lezama, A., Vilanova, E., Ramírez-Angulo, H., Higuchi, N., Neill, D.A., Silveira, M.,
744 Ferreira, L., Aymard C., G.A., Malhi, Y., Phillips, O.L., Lloyd, J., 2014. Analysing Amazonian
745 forest productivity using a new individual and trait-based model (TFS v.1). Geosci. Model Dev.
746 7, 1251–1269. https://doi.org/10.5194/gmd-7-1251-2014

747 Galbraith, D., Levy, P.E., Sitch, S., Huntingford, C., Cox, P., Williams, M., Meir, P., 2010. Multiple
748 mechanisms of Amazonian forest biomass losses in three dynamic global vegetation models
749 under climate change. New Phytol. 187, 647–665. https://doi.org/10.1111/j.1469-
750 8137.2010.03350.x

751 Gardner, T.A., Barlow, J., Sodhi, N.S., Peres, C.A., 2010. A multi-region assessment of tropical forest
752 biodiversity in a human-modified world. Biol. Conserv. 143, 2293–2300.
753 https://doi.org/10.1016/j.biocon.2010.05.017

754 Gilleland, E., Katz, R.W., 2016. {extRemes} 2.0: An Extreme Value Analysis Package in {R}. J. Stat.
755 Softw. 72, 1–39. https://doi.org/10.18637/jss.v072.i08

756 Guan, K., Pan, M., Li, H., Wolf, A., Wu, J., Medvigy, D., Caylor, K.K., Sheffield, J., Wood, E.F.,
757 Malhi, Y., Liang, M., Kimball, J.S., Saleska, S.R., Berry, J., Joiner, J., Lyapustin, A.I., 2015.
758 Photosynthetic seasonality of global tropical forests constrained by hydroclimate. Nat. Geosci. 8,
759 284–289. https://doi.org/10.1038/ngeo2382

760 Harris, I., Jones, P.D., Osborn, T.J., Lister, D.H., 2014. Updated high-resolution grids of monthly

761 climatic observations - the CRU TS3.10 Dataset. Int. J. Climatol. 34, 623–642.
762 https://doi.org/10.1002/joc.3711

763 Hartig, F., Dislich, C., Wiegand, T., Huth, A., 2014. Technical note: Approximate bayesian
764 parameterization of a process-based tropical forest model. Biogeosciences 11, 1261–1272.
765 https://doi.org/10.5194/bg-11-1261-2014

766 Hartig, F., Dyke, J., Hickler, T., Higgins, S.I., O'Hara, R.B., Scheiter, S., Huth, A., 2012. Connecting
767 dynamic vegetation models to data - an inverse perspective. J. Biogeogr. 39, 2240–2252.
768 https://doi.org/10.1111/j.1365-2699.2012.02745.x

769 Hijmans, R.J., 2020. raster: Geographic Data Analysis and Modeling.

770 Hijmans, R.J., 2019. geosphere: Spherical Trigonometry.

771 Huang, S.-C., Lin, Y.-C., Liu, K.-F., Chen, C.-T., 2011. Microplate method for plant total nitrogen and
772 phosphorus analysis. Taiwan. J. Agric. Chem. Food Sci. 49, 19–25.

773 Huber, N., Bugmann, H., Lafond, V., 2018. Global sensitivity analysis of a dynamic vegetation model:
774 Model sensitivity depends on successional time, climate and competitive interactions. Ecol.
775 Modell. 368, 377–390. https://doi.org/10.1016/j.ecolmodel.2017.12.013

776 Ibanez, T., Keppel, G., Menkes, C., Gillespie, T.W., Lengaigne, M., Rivas-torres, M.M.G., Birnbaum,
777 P., Mangeas, M., Rivas, G., Birnbaum, P., 2019. Globally consistent impact of tropical cyclones
778 on the structure of tropical and subtropical forests. J. Ecol. 107, 279–292.
779 https://doi.org/10.1111/1365-2745.13039

780 Ichii, K., Suzuki, T., Kato, T., Ito, A., Hajima, T., Ueyama, M., Sasai, T., Hirata, R., Saigusa, N.,
781 Ohtani, Y., Takagi, K., 2010. Multi-model analysis of terrestrial carbon cycles in Japan:
782 Limitations and implications of model calibration using eddy flux observations. Biogeosciences

783 7, 2061–2081. https://doi.org/10.5194/bg-7-2061-2010

784 Iida, Y., Kohyama, T.S., Swenson, N.G., Su, S.-H., Chen, C.-T., Chiang, J.-M., Sun, I.-F., 2014.
785 Linking functional traits and demographic rates in a subtropical tree community: The importance
786 of size dependency. J. Ecol. 102, 641–650. https://doi.org/10.1111/1365-2745.12221

787 Joetzjer, E., Pillet, M., Ciais, P., Barbier, N., Chave, J., Schlund, M., Maignan, F., Barichivich, J.,
788 Luyssaert, S., Hérault, B., von Poncet, F., Poulter, B., 2017. Assimilating satellite-based canopy
789 height within an ecosystem model to estimate aboveground forest biomass. Geophys. Res. Lett.
790 44, 6823–6832. https://doi.org/10.1002/2017GL074150

791 Johnson, M.O., Galbraith, D., Gloor, M., De Deurwaerder, H., Guimberteau, M., Rammig, A.,
792 Thonicke, K., Verbeeck, H., von Randow, C., Monteagudo, A., Phillips, O.L., Brienen, R.J.W.,
793 Feldpausch, T.R., Lopez Gonzalez, G., Fauset, S., Quesada, C.A., Christoffersen, B., Ciais, P.,
794 Sampaio, G., Kruijt, B., Meir, P., Moorcroft, P., Zhang, K., Alvarez-Davila, E., Alves de
795 Oliveira, A., Amaral, I., Andrade, A., Aragao, L.E.O.C., Araujo-Murakami, A., Arets, E.J.M.M.,
796 Arroyo, L., Aymard, G.A., Baraloto, C., Barroso, J., Bonal, D., Boot, R., Camargo, J., Chave, J.,
797 Cogollo, A., Cornejo Valverde, F., Lola da Costa, A.C., Di Fiore, A., Ferreira, L., Higuchi, N.,
798 Honorio, E.N., Killeen, T.J., Laurance, S.G., Laurance, W.F., Licona, J., Lovejoy, T., Malhi, Y.,
799 Marimon, B., Marimon, B.H., Matos, D.C.L., Mendoza, C., Neill, D.A., Pardo, G., Peña-Claros,
800 M., Pitman, N.C.A., Poorter, L., Prieto, A., Ramirez-Angulo, H., Roopsind, A., Rudas, A.,
801 Salomao, R.P., Silveira, M., Stropp, J., ter Steege, H., Terborgh, J., Thomas, R., Toledo, M.,
802 Torres-Lezama, A., van der Heijden, G.M.F., Vasquez, R., Guimarães Vieira, I.C., Vilanova, E.,
803 Vos, V.A., Baker, T.R., 2016. Variation in stem mortality rates determines patterns of above-
804 ground biomass in Amazonian forests: implications for dynamic global vegetation models. Glob.
805 Chang. Biol. 22, 3996–4013. https://doi.org/10.1111/gcb.13315

Jucker, T., Caspersen, J., Chave, J., Antin, C., Barbier, N., Bongers, F., Dalponte, M., van Ewijk, K.Y., Forrester, D.I., Haeni, M., Higgins, S.I., Holdaway, R.J., Iida, Y., Lorimer, C., Marshall, P.L., Momo, S., Moncrieff, G.R., Ploton, P., Poorter, L., Rahman, K.A., Schlund, M., Sonké, B., Sterck, F.J., Trugman, A.T., Usoltsev, V.A., Vanderwel, M.C., Waldner, P., Wedeux, B.M.M., Wirth, C., Wöll, H., Woods, M., Xiang, W., Zimmermann, N.E., Coomes, D.A., 2017. Allometric equations for integrating remote sensing imagery into forest monitoring programmes. Glob. Chang. Biol. 23, 177–190. https://doi.org/10.1111/gcb.13388

Kalnay, E., Kanamitsu, M., Kistler, R., Collins, W., Deaven, D., Gandin, L., Iredell, M., Saha, S., White, G., Woollen, J., Zhu, Y., Chelliah, M., Ebisuzaki, W., Higgins, W., Janowiak, J., Mo, K.C., Ropelewski, C., Wang, J., Leetmass, A., Reynolds, R., Jenne, R., Joseph, D., 1996. The NCEP/NCAR 40-year Reanalysis Project. Bull. Am. Meteorol. Soc. 77, 437–471.

Kassambara, A., 2020. ggpubr: "ggplot2" Based Publication Ready Plots.

Kattge, J., Bönisch, G., Díaz, S., Lavorel, S., Prentice, I.C., Leadley, P., Tautenhahn, S., Werner, G.D.A., Aakala, T., Abedi, M., Acosta, A.T.R., Adamidis, G.C., Adamson, K., Aiba, M., Albert, C.H., Alcántara, J.M., Alcázar C, C., Aleixo, I., Ali, H., Amiaud, B., Ammer, C., Amoroso, M.M., Anand, M., Anderson, C., Anten, N., Antos, J., Apgaua, D.M.G., Ashman, T.L., Asmara, D.H., Asner, G.P., Aspinwall, M., Atkin, O., Aubin, I., Baastrup-Spohr, L., Bahalkeh, K., Bahn, M., Baker, T., Baker, W.J., Bakker, J.P., Baldocchi, D., Baltzer, J., Banerjee, A., Baranger, A., Barlow, J., Barneche, D.R., Baruch, Z., Bastianelli, D., Battles, J., Bauerle, W., Bauters, M., Bazzato, E., Beckmann, M., Beeckman, H., Beierkuhnlein, C., Bekker, R., Belfry, G., Belluau, M., Beloiu, M., Benavides, R., Benomar, L., Berdugo-Lattke, M.L., Berenguer, E., Bergamin, R., Bergmann, J., Bergmann Carlucci, M., Berner, L., Bernhardt-Römermann, M., Bigler, C., Bjorkman, A.D., Blackman, C., Blanco, C., Blonder, B., Blumenthal, D., Bocanegra-González,

K.T., Boeckx, P., Bohlman, S., Böhning-Gaese, K., Boisvert-Marsh, L., Bond, W., Bond-Lamberty, B., Boom, A., Boonman, C.C.F., Bordin, K., Boughton, E.H., Boukili, V., Bowman, D.M.J.S., Bravo, S., Brendel, M.R., Broadley, M.R., Brown, K.A., Bruelheide, H., Brumnich, F., Bruun, H.H., Bruy, D., Buchanan, S.W., Bucher, S.F., Buchmann, N., Buitenwerf, R., Bunker, D.E., Bürger, J., Burrascano, S., Burslem, D.F.R.P., Butterfield, B.J., Byun, C., Marques, M., Scalon, M.C., Caccianiga, M., Cadotte, M., Cailleret, M., Camac, J., Camarero, J.J., Campany, C., Campetella, G., Campos, J.A., Cano-Arboleda, L., Canullo, R., Carbognani, M., Carvalho, F., Casanoves, F., Castagneyrol, B., Catford, J.A., Cavender-Bares, J., Cerabolini, B.E.L., Cervellini, M., Chacón-Madrigal, E., Chapin, K., Chapin, F.S., Chelli, S., Chen, S.C., Chen, A., Cherubini, P., Chianucci, F., Choat, B., Chung, K.S., Chytrý, M., Ciccarelli, D., Coll, L., Collins, C.G., Conti, L., Coomes, D.A., Cornelissen, J.H.C., Cornwell, W.K., Corona, P., Coyea, M., Craine, J., Craven, D., Cromsigt, J.P.G.M., Csecserits, A., Cufar, K., Cuntz, M., da Silva, A.C., Dahlin, K.M., Dainese, M., Dalke, I., Dalle Fratte, M., Dang-Le, A.T., Danihelka, J., Dannoura, M., Dawson, S., de Beer, A.J., De Frutos, A., De Long, J.R., Dechant, B., Delagrange, S., Delpierre, N., Derroire, G., Dias, A.S., Diaz-Toribio, M.H., Dimitrakopoulos, P.G., Dobrowolski, M., Doktor, D., Dřevojan, P., Dong, N., Dransfield, J., Dressler, S., Duarte, L., Ducouret, E., Dullinger, S., Durka, W., Duursma, R., Dymova, O., E-Vojtkó, A., Eckstein, R.L., Ejtehadi, H., Elser, J., Emilio, T., Engemann, K., Erfanian, M.B., Erfmeier, A., Esquivel-Muelbert, A., Esser, G., Estiarte, M., Domingues, T.F., Fagan, W.F., Fagúndez, J., Falster, D.S., Fan, Y., Fang, J., Farris, E., Fazlioglu, F., Feng, Y., Fernandez-Mendez, F., Ferrara, C., Ferreira, J., Fidelis, A., Finegan, B., Firn, J., Flowers, T.J., Flynn, D.F.B., Fontana, V., Forey, E., Forgiarini, C., François, L., Frangipani, M., Frank, D., Frenette-Dussault, C., Freschet, G.T., Fry, E.L., Fyllas, N.M., Mazzochini, G.G., Gachet, S., Gallagher, R., Ganade, G., Ganga, F., García-Palacios, P.,

Gargaglione, V., Garnier, E., Garrido, J.L., de Gasper, A.L., Gea-Izquierdo, G., Gibson, D., Gillison, A.N., Giroldo, A., Glasenhardt, M.C., Gleason, S., Gliesch, M., Goldberg, E., Göldel, B., Gonzalez-Akre, E., Gonzalez-Andujar, J.L., González-Melo, A., González-Robles, A., Graae, B.J., Granda, E., Graves, S., Green, W.A., Gregor, T., Gross, N., Guerin, G.R., Günther, A., Gutiérrez, A.G., Haddock, L., Haines, A., Hall, J., Hambuckers, A., Han, W., Harrison, S.P., Hattingh, W., Hawes, J.E., He, T., He, P., Heberling, J.M., Helm, A., Hempel, S., Hentschel, J., Hérault, B., Hereş, A.M., Herz, K., Heuertz, M., Hickler, T., Hietz, P., Higuchi, P., Hipp, A.L., Hirons, A., Hock, M., Hogan, J.A., Holl, K., Honnay, O., Hornstein, D., Hou, E., Hough-Snee, N., Hovstad, K.A., Ichie, T., Igić, B., Illa, E., Isaac, M., Ishihara, M., Ivanov, L., Ivanova, L., Iversen, C.M., Izquierdo, J., Jackson, R.B., Jackson, B., Jactel, H., Jagodzinski, A.M., Jandt, U., Jansen, S., Jenkins, T., Jentsch, A., Jespersen, J.R.P., Jiang, G.F., Johansen, J.L., Johnson, D., Jokela, E.J., Joly, C.A., Jordan, G.J., Joseph, G.S., Junaedi, D., Junker, R.R., Justes, E., Kabzems, R., Kane, J., Kaplan, Z., Kattenborn, T., Kavelenova, L., Kearsley, E., Kempel, A., Kenzo, T., Kerkhoff, A., Khalil, M.I., Kinlock, N.L., Kissling, W.D., Kitajima, K., Kitzberger, T., Kjøller, R., Klein, T., Kleyer, M., Klimešová, J., Klipel, J., Kloeppel, B., Klotz, S., Knops, J.M.H., Kohyama, T., Koike, F., Kollmann, J., Komac, B., Komatsu, K., König, C., Kraft, N.J.B., Kramer, K., Kreft, H., Kühn, I., Kumarathunge, D., Kuppler, J., Kurokawa, H., Kurosawa, Y., Kuyah, S., Laclau, J.P., Lafleur, B., Lallai, E., Lamb, E., Lamprecht, A., Larkin, D.J., Laughlin, D., Le Bagousse-Pinguet, Y., le Maire, G., le Roux, P.C., le Roux, E., Lee, T., Lens, F., Lewis, S.L., Lhotsky, B., Li, Y., Li, X., Lichstein, J.W., Liebergesell, M., Lim, J.Y., Lin, Y.S., Linares, J.C., Liu, C., Liu, D., Liu, U., Livingstone, S., Llusià, J., Lohbeck, M., López-García, Á., Lopez-Gonzalez, G., Lososová, Z., Louault, F., Lukács, B.A., Lukeš, P., Luo, Y., Lussu, M., Ma, S., Maciel Rabelo Pereira, C., Mack, M., Maire, V., Mäkelä, A., Mäkinen, H., Malhado, A.C.M.,

Mallik, A., Manning, P., Manzoni, S., Marchetti, Z., Marchino, L., Marcilio-Silva, V., Marcon, E., Marignani, M., Markesteijn, L., Martin, A., Martínez-Garza, C., Martínez-Vilalta, J., Mašková, T., Mason, K., Mason, N., Massad, T.J., Masse, J., Mayrose, I., McCarthy, J., McCormack, M.L., McCulloh, K., McFadden, I.R., McGill, B.J., McPartland, M.Y., Medeiros, J.S., Medlyn, B., Meerts, P., Mehrabi, Z., Meir, P., Melo, F.P.L., Mencuccini, M., Meredieu, C., Messier, J., Mészáros, I., Metsaranta, J., Michaletz, S.T., Michelaki, C., Migalina, S., Milla, R., Miller, J.E.D., Minden, V., Ming, R., Mokany, K., Moles, A.T., Molnár, A., Molofsky, J., Molz, M., Montgomery, R.A., Monty, A., Moravcová, L., Moreno-Martínez, A., Moretti, M., Mori, A.S., Mori, S., Morris, D., Morrison, J., Mucina, L., Mueller, S., Muir, C.D., Müller, S.C., Munoz, F., Myers-Smith, I.H., Myster, R.W., Nagano, M., Naidu, S., Narayanan, A., Natesan, B., Negoita, L., Nelson, A.S., Neuschulz, E.L., Ni, J., Niedrist, G., Nieto, J., Niinemets, Ü., Nolan, R., Nottebrock, H., Nouvellon, Y., Novakovskiy, A., Nystuen, K.O., O'Grady, A., O'Hara, K., O'Reilly-Nugent, A., Oakley, S., Oberhuber, W., Ohtsuka, T., Oliveira, R., Öllerer, K., Olson, M.E., Onipchenko, V., Onoda, Y., Onstein, R.E., Ordonez, J.C., Osada, N., Ostonen, I., Ottaviani, G., Otto, S., Overbeck, G.E., Ozinga, W.A., Pahl, A.T., Paine, C.E.T., Pakeman, R.J., Papageorgiou, A.C., Parfionova, E., Pärtel, M., Patacca, M., Paula, S., Paule, J., Pauli, H., Pausas, J.G., Peco, B., Penuelas, J., Perea, A., Peri, P.L., Petisco-Souza, A.C., Petraglia, A., Petritan, A.M., Phillips, O.L., Pierce, S., Pillar, V.D., Pisek, J., Pomogaybin, A., Poorter, H., Portsmuth, A., Poschlod, P., Potvin, C., Pounds, D., Powell, A.S., Power, S.A., Prinzing, A., Puglielli, G., Pyšek, P., Raevel, V., Rammig, A., Ransijn, J., Ray, C.A., Reich, P.B., Reichstein, M., Reid, D.E.B., Réjou-Méchain, M., de Dios, V.R., Ribeiro, S., Richardson, S., Riibak, K., Rillig, M.C., Riviera, F., Robert, E.M.R., Roberts, S., Robroek, B., Roddy, A., Rodrigues, A.V., Rogers, A., Rollinson, E., Rolo, V., Römermann, C., Ronzhina, D., Roscher, C., Rosell, J.A.,

898 Rosenfield, M.F., Rossi, C., Roy, D.B., Royer-Tardif, S., Rüger, N., Ruiz-Peinado, R., Rumpf,
899 S.B., Rusch, G.M., Ryo, M., Sack, L., Saldaña, A., Salgado-Negret, B., Salguero-Gomez, R.,
900 Santa-Regina, I., Santacruz-García, A.C., Santos, J., Sardans, J., Schamp, B., Scherer-Lorenzen,
901 M., Schleuning, M., Schmid, B., Schmidt, M., Schmitt, S., Schneider, J. V., Schowanek, S.D.,
902 Schrader, J., Schrodt, F., Schuldt, B., Schurr, F., Selaya Garvizu, G., Semchenko, M., Seymour,
903 C., Sfair, J.C., Sharpe, J.M., Sheppard, C.S., Sheremetiev, S., Shiodera, S., Shipley, B., Shovon,
904 T.A., Siebenkäs, A., Sierra, C., Silva, V., Silva, M., Sitzia, T., Sjöman, H., Slot, M., Smith, N.G.,
905 Sodhi, D., Soltis, P., Soltis, D., Somers, B., Sonnier, G., Sørensen, M.V., Sosinski, E.E.,
906 Soudzilovskaia, N.A., Souza, A.F., Spasojevic, M., Sperandii, M.G., Stan, A.B., Stegen, J.,
907 Steinbauer, K., Stephan, J.G., Sterck, F., Stojanovic, D.B., Strydom, T., Suarez, M.L., Svenning,
908 J.C., Svitková, I., Svitok, M., Svoboda, M., Swaine, E., Swenson, N., Tabarelli, M., Takagi, K.,
909 Tappeiner, U., Tarifa, R., Tauugourdeau, S., Tavsanoglu, C., te Beest, M., Tedersoo, L.,
910 Thiffault, N., Thom, D., Thomas, E., Thompson, K., Thornton, P.E., Thuiller, W., Tichý, L.,
911 Tissue, D., Tjoelker, M.G., Tng, D.Y.P., Tobias, J., Török, P., Tarin, T., Torres-Ruiz, J.M.,
912 Tóthmérész, B., Treurnicht, M., Trivellone, V., Trolliet, F., Trotsiuk, V., Tsakalos, J.L.,
913 Tsiripidis, I., Tysklind, N., Umehara, T., Usoltsev, V., Vadeboncoeur, M., Vaezi, J., Valladares,
914 F., Vamosi, J., van Bodegom, P.M., van Breugel, M., Van Cleemput, E., van de Weg, M., van
915 der Merwe, S., van der Plas, F., van der Sande, M.T., van Kleunen, M., Van Meerbeek, K.,
916 Vanderwel, M., Vanselow, K.A., Vårhammar, A., Varone, L., Vasquez Valderrama, M.Y.,
917 Vassilev, K., Vellend, M., Veneklaas, E.J., Verbeeck, H., Verheyen, K., Vibrans, A., Vieira, I.,
918 Villacís, J., Violle, C., Vivek, P., Wagner, K., Waldram, M., Waldron, A., Walker, A.P., Waller,
919 M., Walther, G., Wang, H., Wang, F., Wang, W., Watkins, H., Watkins, J., Weber, U., Weedon,
920 J.T., Wei, L., Weigelt, P., Weiher, E., Wells, A.W., Wellstein, C., Wenk, E., Westoby, M.,

Westwood, A., White, P.J., Whitten, M., Williams, M., Winkler, D.E., Winter, K., Womack, C., Wright, I.J., Wright, S.J., Wright, J., Pinho, B.X., Ximenes, F., Yamada, T., Yamaji, K., Yanai, R., Yankov, N., Yguel, B., Zanini, K.J., Zanne, A.E., Zelený, D., Zhao, Y.P., Zheng, Jingming, Zheng, Ji, Ziemińska, K., Zirbel, C.R., Zizka, G., Zo-Bi, I.C., Zotz, G., Wirth, C., 2020. TRY plant trait database – enhanced coverage and open access. Glob. Chang. Biol. 26, 119–188. https://doi.org/10.1111/gcb.14904

Kistler, R., Kalnay, E., Collins, W., Saha, S., White, G., Woollen, J., Chelliah, M., Ebisuzaki, W., Kanamitsu, M., Kousky, V., Van Den Dool, H., Jenne, R., Fiorino, M., 2001. The NCEP-NCAR 50-year reanalysis: Monthly means CD-ROM and documentation. Bull. Am. Meteorol. Soc. 82, 247–267. https://doi.org/10.1175/1520-0477(2001)082<0247:TNNYRM>2.3.CO;2

Lagarrigues, G., Jabot, F., Lafond, V., Courbaud, B., 2015. Approximate Bayesian computation to recalibrate individual-based models with population data: Illustration with a forest simulation model. Ecol. Modell. 306, 278–286. https://doi.org/10.1016/j.ecolmodel.2014.09.023

Lehmann, S., Huth, A., 2015. Fast calibration of a dynamic vegetation model with minimum observation data. Ecol. Modell. 301, 98–105. https://doi.org/10.1016/j.ecolmodel.2015.01.013

Lin, T., Vadeboncoeur, M.A., Hamburg, S.P., Lin, K.-C., Wang, L., Chang, C., Hsia, Y., Mcmullen, C.M.M., Liu, C., 2011. Typhoon Disturbance and Forest Dynamics: Lessons from a Northwest Pacific Subtropical Forest. Ecosystems 14, 127–143. https://doi.org/10.1007/s10021-010-9399-1

Loubota Panzou, G.J., Fayolle, A., Jucker, T., Phillips, O.L., Bohlman, S., Banin, L.F., Lewis, S.L., Affum-Baffoe, K., Alves, L.F., Antin, C., Arets, E., Arroyo, L., Baker, T.R., Barbier, N., Beeckman, H., Berger, U., Bocko, Y.E., Bongers, F., Bowers, S., Brade, T., Brondizio, E.S., Chantrain, A., Chave, J., Compaore, H., Coomes, D.A., Diallo, A., Dias, A.S., Dimobe, K.,

943 Djagbletey, G.D., Domingues, T., Doucet, J.L., Drouet, T., Forni, E., Godlee, J.L., Goodman,
944 R.C., Gourlet-Fleury, S., Hien, F., Iida, Y., Ilondea, B.A., Ilunga Muledi, J., Jacques, P., Kuyah,
945 S., López-Portillo, J., Loumeto, J.J., Marimon-Junior, B.H., Marimon, B.S., Mensah, S.,
946 Mitchard, E.T.A., Moncrieff, G.R., Narayanan, A., O'Brien, S.T., Ouedraogo, K., Palace, M.W.,
947 Pelissier, R., Ploton, P., Poorter, L., Ryan, C.M., Saiz, G., dos Santos, K., Schlund, M., Sellan,
948 G., Sonke, B., Sterck, F., Thibaut, Q., Van Hoef, Y., Veenendaal, E., Vovides, A.G., Xu, Y.,
949 Yao, T.L., Feldpausch, T.R., 2021. Pantropical variability in tree crown allometry. Glob. Ecol.
950 Biogeogr. 30, 459–475. https://doi.org/10.1111/geb.13231

951 Ma, J., Shugart, H.H., Yan, X., Cao, C., Wu, S., Fang, J., 2017. Evaluating carbon fluxes of global
952 forest ecosystems by using an individual tree-based model FORCCHN. Sci. Total Environ. 586,
953 939–951. https://doi.org/10.1016/j.scitotenv.2017.02.073

954 Madani, N., Parazoo, N.C., 2020. Global Monthly GPP from an Improved Light Use Efficiency Model,
955 1982-2016 [WWW Document]. URL https://daac.ornl.gov/cgi-bin/dsviewer.pl?ds_id=1789
956 (accessed 12.14.20).

957 Magnabosco Marra, D., Trumbore, S.E., Higuchi, N., Ribeiro, G.H.P.M., Negrón-Juárez, R.I.,
958 Holzwarth, F., Rifai, S.W., dos Santos, J., Lima, A.J.N., Kinupp, V.F., Chambers, J.Q., Wirth,
959 C., 2018. Windthrows control biomass patterns and functional composition of Amazon forests.
960 Glob. Chang. Biol. 24, 5867–5881. https://doi.org/10.1111/gcb.14457

961 Malhi, Y., Aragão, L.E.O.C., Galbraith, D., Huntingford, C., Fisher, R., Zelazowski, P., Sitch, S.,
962 Mcsweeney, C., Meir, P., 2009. Exploring the likelihood and mechanism of a climate-change-
963 induced dieback of the. PNAS 106, 20610–20615.

964 Malhi, Y., Doughty, C.E., Goldsmith, G.R., Metcalfe, D.B., Girardin, C.A.J., Marthews, T.R., del

965 Aguila-Pasquel, J., Aragão, L.E.O.C., Araujo-Murakami, A., Brando, P., da Costa, A.C.L., Silva-
966 Espejo, J.E., Farfán Amézquita, F., Galbraith, D.R., Quesada, C.A., Rocha, W., Salinas-Revilla,
967 N., Silvério, D., Meir, P., Phillips, O.L., 2015. The linkages between photosynthesis,
968 productivity, growth and biomass in lowland Amazonian forests. Glob. Chang. Biol. 21, 2283–
969 2295. https://doi.org/10.1111/gcb.12859

970 Maréchaux, I., Chave, J., 2017. An individual-based forest model to jointly simulate carbon and tree
971 diversity in Amazonia: description and applications. Ecol. Monogr. 87, 632–664.
972 https://doi.org/10.1002/ecm.1271

973 Maréchaux, I., Langerwisch, F., Huth, A., Bugmann, H., Morin, X., Reyer, C.P.O., Seidl, R., Collalti,
974 A., Dantas de Paula, M., Fischer, R., Gutsch, M., Lexer, M.J., Lischke, H., Rammig, A., Rödig,
975 E., Sakschewski, B., Taubert, F., Thonicke, K., Vacchiano, G., Bohn, F.J., 2021. Tackling
976 unresolved questions in forest ecology: The past and future role of simulation models. Ecol.
977 Evol. 1–25. https://doi.org/10.1002/ece3.7391

978 McDowell, N., Allen, C.D., Anderson-Teixeira, K.J., Brando, P., Brienen, R., Chambers, J.,
979 Christoffersen, B., Davies, S., Doughty, C., Duque, A., Espirito-Santo, F., Fisher, R.A., Fontes,
980 C.G., Galbraith, D., Goodsman, D., Grossiord, C., Hartmann, H., Holm, J., Johnson, D.J.,
981 Kassim, A.R., Keller, M., Koven, C., Kueppers, L., Kumagai, T., Malhi, Y., McMahon, S.M.,
982 Mencuccini, M., Meir, P., Moorcroft, P., Muller-Landau, H.C., Phillips, O.L., Powell, T., Sierra,
983 C.A., Sperry, J., Warren, J., Xu, C., Xu, X., 2018. Drivers and mechanisms of tree mortality in
984 moist tropical forests. New Phytol. 219, 851–869. https://doi.org/10.1111/nph.15027

985 Medlyn, B.E., De Kauwe, M.G., Zaehle, S., Walker, A.P., Duursma, R.A., Luus, K., Mishurov, M.,
986 Pak, B., Smith, B., Wang, Y.P., Yang, X., Crous, K.Y., Drake, J.E., Gimeno, T.E., Macdonald,

C.A., Norby, R.J., Power, S.A., Tjoelker, M.G., Ellsworth, D.S., 2016. Using models to guide field experiments: a priori predictions for the CO2 response of a nutrient- and water-limited native Eucalypt woodland. Glob. Chang. Biol. 22, 2834–2851. https://doi.org/10.1111/gcb.13268

Medlyn, B.E., Duursma, R.A., Eamus, D., Ellsworth, D.S., Prentice, I.C., Barton, C.V.M., Crous, K.Y., De Angelis, P., Freeman, M., Wingate, L., 2011. Reconciling the optimal and empirical approaches to modelling stomatal conductance. Glob. Chang. Biol. 17, 2134–2144. https://doi.org/10.1111/j.1365-2486.2010.02375.x

Mercado, L.M., Lloyd, J., Dolman, A.J., Sitch, S., Patiño, S., 2009. Modelling basin-wide variations in Amazon forest productivity - Part 1: Model calibration, evaluation and upscaling functions for canopy photosynthesis. Biogeosciences 6, 1247–1272. https://doi.org/10.5194/bg-6-1247-2009

Merganičová, K., Merganič, J., Lehtonen, A., Vacchiano, G., Sever, M.Z.O., Augustynczik, A.L.D., Grote, R., Kyselová, I., Mäkelä, A., Yousefpour, R., Krejza, J., Collalti, A., Reyer, C.P.O., 2019. Forest carbon allocation modelling under climate change. Tree Physiol. 39, 1937–1960. https://doi.org/10.1093/treephys/tpz105

Mitchard, E.T.A., 2018. The tropical forest carbon cycle and climate change. Nature 559, 527–534. https://doi.org/10.1038/s41586-018-0300-2

Molto, Q., Hérault, B., Boreux, J.J., Daullet, M., Rousteau, A., Rossi, V., 2014. Predicting tree heights for biomass estimates in tropical forests - A test from French Guiana. Biogeosciences 11, 3121–3130. https://doi.org/10.5194/bg-11-3121-2014

Monteith, J., Unsworth, M., 2008. Principles of environmental physics: plants, animals, and the atmosphere, 3rd ed. Academic Press.

Negrón-Juárez, R.I., Koven, C.D., Riley, W.J., Knox, R.G., Chambers, J.Q., 2015. Observed

allocations of productivity and biomass, and turnover times in tropical forests are not accurately represented in CMIP5 Earth system models. Environ. Res. Lett. 10. https://doi.org/10.1088/1748-9326/10/6/064017

Pappas, C., Fatichi, S., Burlando, P., 2016. Modeling terrestrial carbon and water dynamics across climatic gradients: Does plant trait diversity matter? New Phytol. 209, 137–151. https://doi.org/10.1111/nph.13590

Pappas, C., Fatichi, S., Leuzinger, S., Wolf, A., Burlando, P., 2013. Sensitivity analysis of a process-based ecosystem model: Pinpointing parameterization and structural issues. J. Geophys. Res. Biogeosciences 118, 505–528. https://doi.org/10.1002/jgrg.20035

Pérez-Harguindeguy, N., Díaz, S., Garnier, E., Lavorel, S., Poorter, H., Jaureguiberry, P., Bret-Harte, M.S., Cornwell, W.K., Craine, J.M., Gurvich, D.E., Urcelay, C., Veneklaas, E.J., Reich, P.B., Poorter, L., Wright, I.J., Ray, P., Enrico, L., Pausas, J.G., De Vos, A.C., Buchmann, N., Funes, G., Quétier, F., Hodgson, J.G., Thompson, K., Morgan, H.D., Ter Steege, H., Van Der Heijden, M.G.A., Sack, L., Blonder, B., Poschlod, P., Vaieretti, M. V., Conti, G., Staver, A.C., Aquino, S., Cornelissen, J.H.C., 2013. New handbook for standardised measurement of plant functional traits worldwide. Aust. J. Bot. 61, 167–234. https://doi.org/10.1071/BT12225

Peterson, C.J., Ribeiro, G.H.P. de M., Negrón-Juárez, R., Marra, D.M., Chambers, J.Q., Higuchi, N., Lima, A., Cannon, J.B., 2019. Critical wind speeds suggest wind could be an important disturbance agent in Amazonian forests. For. An Int. J. For. Res. 92, 444–459. https://doi.org/10.1093/forestry/cpz025

Pierce, D., 2019. ncdf4: Interface to Unidata netCDF (Version 4 or Earlier) Format Data Files.

Poorter, L., van der Sande, M.T., Arets, E.J.M.M., Ascarrunz, N., Enquist, B., Finegan, B., Licona,

J.C., Martínez-Ramos, M., Mazzei, L., Meave, J.A., Muñoz, R., Nytch, C.J., de Oliveira, A.A., Pérez-García, E.A., Prado-Junior, J., Rodríguez-Velázques, J., Ruschel, A.R., Salgado-Negret, B., Schiavini, I., Swenson, N.G., Tenorio, E.A., Thompson, J., Toledo, M., Uriarte, M., Hout, P. van der, Zimmerman, J.K., Peña-Claros, M., 2017. Biodiversity and climate determine the functioning of Neotropical forests. Glob. Ecol. Biogeogr. 26, 1423–1434. https://doi.org/10.1111/geb.12668

Prentice, I.C., Liang, X., Medlyn, B.E., Wang, Y.P., 2015. Reliable, robust and realistic: The three R's of next-generation land-surface modelling. Atmos. Chem. Phys. 15, 5987–6005. https://doi.org/10.5194/acp-15-5987-2015

Pretzsch, H., 2019. The effect of tree crown allometry on community dynamics in mixed-species stands versus monocultures. A review and perspectives for modeling and silvicultural regulation. Forests 10. https://doi.org/10.3390/f10090810

Pugh, T.A.M., Arneth, A., Kautz, M., Poulter, B., Smith, B., 2019. Important role of forest disturbances in the global biomass turnover and carbon sinks. Nat. Geosci. 12, 730–735. https://doi.org/10.1038/s41561-019-0427-2

R Core Team, 2019. R: A Language and Environment for Statistical Computing.

Rejou-Mechain, M., Tanguy, A., Piponiot, C., Chave, J., Herault, B., 2017. BIOMASS : an {R} package for estimating above-ground biomass and its uncertainty in tropical forests. Methods Ecol. Evol. 8. https://doi.org/10.1111/2041-210X.12753

Restrepo-Coupe, N., Levine, N.M., Christoffersen, B.O., Albert, L.P., Wu, J., Costa, M.H., Galbraith, D., Imbuzeiro, H., Martins, G., da Araujo, A.C., Malhi, Y.S., Zeng, X., Moorcroft, P., Saleska, S.R., 2017. Do dynamic global vegetation models capture the seasonality of carbon fluxes in the

Amazon basin? A data-model intercomparison. Glob. Chang. Biol. 23, 191–208. https://doi.org/10.1111/gcb.13442

Reyer, C., 2015. Forest productivity under environmental change—A review of stand-scale modeling studies. Curr. For. Reports 1, 53–68. https://doi.org/10.1007/s40725-015-0009-5

Rödig, E., Cuntz, M., Heinke, J., Rammig, A., Huth, A., 2017. Spatial heterogeneity of biomass and forest structure of the Amazon rain forest: Linking remote sensing, forest modelling and field inventory. Glob. Ecol. Biogeogr. 26, 1292–1302. https://doi.org/10.1111/geb.12639

Rödig, E., Cuntz, M., Rammig, A., Fischer, R., Taubert, F., Huth, A., 2018. The importance of forest structure for carbon fluxes of the Amazon rainforest. Environ. Res. Lett. 13. https://doi.org/10.1088/1748-9326/aabc61

Sakschewski, B., von Bloh, W., Boit, A., Rammig, A., Kattge, J., Poorter, L., Peñuelas, J., Thonicke, K., 2015. Leaf and stem economics spectra drive diversity of functional plant traits in a dynamic global vegetation model. Glob. Chang. Biol. 21, 2711–2725. https://doi.org/10.1111/gcb.12870

Sato, H., Itoh, A., Kohyama, T., 2007. SEIB-DGVM: A new Dynamic Global Vegetation Model using a spatially explicit individual-based approach. Ecol. Modell. 200, 279–307. https://doi.org/10.1016/j.ecolmodel.2006.09.006

Schippers, P., Vlam, M., Zuidema, P.A., Sterck, F., 2015. Sapwood allocation in tropical trees: A test of hypotheses. Funct. Plant Biol. 42, 697–709. https://doi.org/10.1071/FP14127

Schulzweida, U., 2019. CDO User Guide (Version 1.9.8) [WWW Document]. https://doi.org/10.5281/zenodo.3539275

Seidl, R., Fernandes, P.M., Fonseca, T.F., Gillet, F., Jönsson, A.M., Merganičová, K., Netherer, S., Arpaci, A., Bontemps, J.D., Bugmann, H., González-Olabarria, J.R., Lasch, P., Meredieu, C.,

1075 Moreira, F., Schelhaas, M.J., Mohren, F., 2011. Modelling natural disturbances in forest
1076 ecosystems: A review. Ecol. Modell. 222, 903–924.
1077 https://doi.org/10.1016/j.ecolmodel.2010.09.040

1078 Seidl, R., Rammer, W., Blennow, K., 2014. Simulating wind disturbance impacts on forest landscapes:
1079 Tree-level heterogeneity matters. Environ. Model. Softw. 51, 1–11.
1080 https://doi.org/10.1016/j.envsoft.2013.09.018

1081 Shugart, H.H., 1984. A theory of forest dynamics. The ecological implications of forest succession
1082 models. Springer Verlag, New York.

1083 Shugart, H.H., Asner, G.P., Fischer, R., Huth, A., Knapp, N., Le Toan, T., Shuman, J.K., 2015.
1084 Computer and remote-sensing infrastructure to enhance large-scale testing of individual-based
1085 forest models. Front. Ecol. Environ. 13, 503–511. https://doi.org/10.1890/140327

1086 Shugart, H.H., Wang, B., Fischer, R., Ma, J., Fang, J., Yan, X., Huth, A., Armstrong, A.H., 2018. Gap
1087 models and their individual-based relatives in the assessment of the consequences of global
1088 change. Environ. Res. Lett. 13. https://doi.org/10.1088/1748-9326/aaaacc

1089 Shuman, J.K., Tchebakova, N.M., Parfenova, E.I., Soja, A.J., Shugart, H.H., Ershov, D., Holcomb, K.,
1090 2015. Forest forecasting with vegetation models across Russia. Can. J. For. Res. 45, 175–184.
1091 https://doi.org/10.1139/cjfr-2014-0138

1092 Stan Development Team, 2016a. Stan Modeling Language Users Guide and Reference Manual,
1093 Version 2.14.0 [WWW Document]. URL http://mc-stan.org

1094 Stan Development Team, 2016b. RStan: the R interface to Stan. R package version 2.14.1. [WWW
1095 Document]. URL http://mc-stan.org

1096 Su, S.-H., Chang-Yang, C., Lu, C., Tsui, C., Lin, T., Lin, C., Chiou, W., Kuan, L., Chen, Z., Hsieh, C.,

2007. Fushan subtropical forest dynamics plot: tree species characteristics and distribution patterns. Taiwan Forestry Research Institute., Taipei.

Sullivan, M.J.P., Lewis, S.L., Affum-Baffoe, K., Castilho, C., Costa, F., Sanchez, A.C., Ewango, C.E.N., Hubau, W., Marimon, B., Monteagudo-Mendoza, A., Qie, L., Sonké, B., Martinez, R.V., Baker, T.R., Brienen, R.J.W., Feldpausch, T.R., Galbraith, D., Gloor, M., Malhi, Y., Aiba, S.I., Alexiades, M.N., Almeida, E.C., De Oliveira, E.A., Dávila, E.Á., Loayza, P.A., Andrade, A., Vieira, S.A., Aragão, L.E.O.C., Araujo-Murakami, A., Arets, E.J.M.M., Arroyo, L., Ashton, P., Gerardo Aymard, C., Baccaro, F.B., Banin, L.F., Baraloto, C., Camargo, P.B., Barlow, J., Barroso, J., Bastin, J.F., Batterman, S.A., Beeckman, H., Begne, S.K., Bennett, A.C., Berenguer, E., Berry, N., Blanc, L., Boeckx, P., Bogaert, J., Bonal, D., Bongers, F., Bradford, M., Brearley, F.Q., Brncic, T., Brown, F., Burban, B., Camargo, J.L., Castro, W., Céron, C., Ribeiro, S.C., Moscoso, V.C., Chave, J., Chezeaux, E., Clark, C.J., De Souza, F.C., Collins, M., Comiskey, J.A., Valverde, F.C., Medina, M.C., Da Costa, L., Dančsák, M., Dargie, G.C., Davies, S., Cardozo, N.D., De Haulleville, T., De Medeiros, M.B., Del Aguila Pasquel, J., Derroire, G., Di Fiore, A., Doucet, J.L., Dourdain, A., Droissart, V., Duque, L.F., Ekoungoulou, R., Elias, F., Erwin, T., Esquivel-Muelbert, A., Fauset, S., Ferreira, J., Llampazo, G.F., Foli, E., Ford, A., Gilpin, M., Hall, J.S., Hamer, K.C., Hamilton, A.C., Harris, D.J., Hart, T.B., Hédl, R., Herault, B., Herrera, R., Higuchi, N., Hladik, A., Coronado, E.H., Huamantupa-Chuquimaco, I., Huasco, W.H., Jeffery, K.J., Jimenez-Rojas, E., Kalamandeen, M., Djuikouo, M.N.K., Kearsley, E., Umetsu, R.K., Kho, L.K., Killeen, T., Kitayama, K., Klitgaard, B., Koch, A., Labrière, N., Laurance, W., Laurance, S., Leal, M.E., Levesley, A., Lima, A.J.N., Lisingo, J., Lopes, A.P., Lopez-Gonzalez, G., Lovejoy, T., Lovett, J.C., Lowe, R., Magnusson, W.E., Malumbres-Olarte, J., Manzatto, Â.G., Marimon, B.H., Marshall, A.R., Marthews, T., De Almeida Reis, S.M.,

Maycock, C., Melgaço, K., Mendoza, C., Metali, F., Mihindou, V., Milliken, W., Mitchard, E.T.A., Morandi, P.S., Mossman, H.L., Nagy, L., Nascimento, H., Neill, D., Nilus, R., Vargas, P.N., Palacios, W., Camacho, N.P., Peacock, J., Pendry, C., Mora, M.C.P., Pickavance, G.C., Pipoly, J., Pitman, N., Playfair, M., Poorter, L., Poulsen, J.R., Poulsen, A.D., Preziosi, R., Prieto, A., Primack, R.B., Ramírez-Angulo, H., Reitsma, J., Réjou-Méchain, M., Correa, Z.R., De Sousa, T.R., Bayona, L.R., Roopsind, A., Rudas, A., Rutishauser, E., Salim, K.A., Salomão, R.P., Schietti, J., Sheil, D., Silva, R.C., Espejo, J.S., Valeria, C.S., Silveira, M., Simo-Droissart, M., Simon, M.F., Singh, J., Shareva, Y.C.S., Stahl, C., Stropp, J., Sukri, R., Sunderland, T., Svátek, M., Swaine, M.D., Swamy, V., Taedoumg, H., Talbot, J., Taplin, J., Taylor, D., Ter Steege, H., Terborgh, J., Thomas, R., Thomas, S.C., Torres-Lezama, A., Umunay, P., Gamarra, L.V., Van Der Heijden, G., Van Der Hout, P., Van Der Meer, P., Van Nieuwstadt, M., Verbeeck, H., Vernimmen, R., Vicentini, A., Vieira, I.C.G., Torre, E.V., Vleminckx, J., Vos, V., Wang, O., White, L.J.T., Willcock, S., Woods, J.T., Wortel, V., Young, K., Zagt, R., Zemagho, L., Zuidema, P.A., Zwerts, J.A., Phillips, O.L., 2020. Long-term thermal sensitivity of earth's tropical forests. Science (80-.). 368, 869–874. https://doi.org/10.1126/science.aaw7578

Townsend, A.R., Asner, G.P., Cleveland, C.C., 2008. The biogeochemical heterogeneity of tropical forests. Trends Ecol. Evol. 23, 424–431. https://doi.org/10.1016/j.tree.2008.04.009

Trugman, A.T., Anderegg, L.D.L., Wolfe, B.T., Birami, B., Ruehr, N.K., Detto, M., Bartlett, M.K., Anderegg, W.R.L., 2019. Climate and plant trait strategies determine tree carbon allocation to leaves and mediate future forest productivity. Glob. Chang. Biol. 25, 3395–3405. https://doi.org/10.1111/gcb.14680

Uriarte, M., Canham, C.D., Thompson, J., Zimmerman, J.K., Murphy, L., Sabat, A.M., Fetcher, N., Haines, B.L., 2009. Natural disturbance and human land use as determinants of tropical forest

dynamics: Results from a forest simulator. Ecol. Monogr. 79, 423–443. https://doi.org/10.1890/08-0707.1

Venables, W.N., Ripley, B.D., 2002. Modern Applied Statistics with S, Fourth. ed. Springer, New York.

Vieilledent, G., Courbaud, B., Kunstler, G., Dhôte, J.F., Clark, J.S., 2010. Individual variability in tree allometry determines light resource allocation in forest ecosystems: A hierarchical Bayesian approach. Oecologia 163, 759–773. https://doi.org/10.1007/s00442-010-1581-9

Viovy, N., 2018. CRUNCEP Version 7 - Atmospheric Forcing Data for the Community Land Model. Research Data Archive at the National Center for Atmospheric Research, Computational and Information Systems Laboratory. [WWW Document]. URL http://rda.ucar.edu/datasets/ds314.3/ (accessed 5.4.17).

Wagner, F.H., Hérault, B., Bonal, D., Stahl, C., Anderson, L.O., Baker, T.R., Sebastian Becker, G., Beeckman, H., Boanerges Souza, D., Cesar Botosso, P., Bowman, D.M.J.S., Bräuning, A., Brede, B., Irving Brown, F., Julio Camarero, J., Camargo, P.B., Cardoso, F.C.G., Carvalho, F.A., Castro, W., Koloski Chagas, R., Chave, J., Chidumayo, E.N., Clark, D.A., Regina Capellotto Costa, F., Couralet, C., Henrique Da Silva Mauricio, P., Dalitz, H., Resende De Castro, V., Milani, J.E.D.F., Consuelo De Oliveira, E., De Souza Arruda, L., Devineau, J.L., Drew, D.M., Dünisch, O., Durigan, G., Elifuraha, E., Fedele, M., Ferreira Fedele, L., Figueiredo Filho, A., Finger, C.A.G., César Franco, A., Jnior, L.F., Galvão, F., Gebrekirstos, A., Gliniars, R., Maurício Lima De Alencastro Graça, P., Griffiths, A.D., Grogan, J., Guan, K., Homeier, J., Raquel Kanieski, M., Khoon Kho, L., Koenig, J., Valerio Kohler, S., Krepkowski, J., Lemos-Filho, J.P., Lieberman, D., Eugene Lieberman, M., Sergio Lisi, C., Longhi Santos, T., Ayala, J.L.L., Eijji

1165 Maeda, E., Malhi, Y., Maria, V.R.B., Marques, M.C.M., Marques, R., Maza Chamba, H.,
1166 Mbwambo, L., Liana Lisboa Melgaço, K., Angela Mendivelso, H., Murphy, B.P., O'Brien, J.J.,
1167 F. Oberbauer, S., Okada, N., Plissier, R., Prior, L.D., Alejandro Roig, F., Ross, M., Rodrigo
1168 Rossatto, D., Rossi, V., Rowland, L., Rutishauser, E., Santana, H., Schulze, M., Selhorst, D.,
1169 Rodrigues Silva, W., Silveira, M., Spannl, S., Swaine, M.D., Toledo, J.J., Miranda Toledo, M.,
1170 Toledo, M., Toma, T., Tomazello Filho, M., Ignacio Valdez Hernández, J., Verbesselt, J.,
1171 Aparecida Vieira, S., Vincent, G., Volkmer De Castilho, C., Volland, F., Worbes, M., Lea
1172 Bolzan Zanon, M., Aragão, L.E.O.C., 2016. Climate seasonality limits leaf carbon assimilation
1173 and wood productivity in tropical forests. Biogeosciences 13, 2537–2562.
1174 https://doi.org/10.5194/bg-13-2537-2016

1175 Wenger, S.J., Olden, J.D., 2012. Assessing transferability of ecological models: An underappreciated
1176 aspect of statistical validation. Methods Ecol. Evol. 3, 260–267. https://doi.org/10.1111/j.2041-
1177 210X.2011.00170.x

1178 Wickham, H., 2020. tidyr: Tidy Messy Data.

1179 Wickham, H., 2016. ggplot2: Elegant Graphics for Data Analysis. Springer-Verlag New York.

1180 Yates, K.L., Bouchet, P.J., Caley, M.J., Mengersen, K., Randin, C.F., Parnell, S., Fielding, A.H.,
1181 Bamford, A.J., Ban, S., Barbosa, A.M., Dormann, C.F., Elith, J., Embling, C.B., Ervin, G.N.,
1182 Fisher, R., Gould, S., Graf, R.F., Gregr, E.J., Halpin, P.N., Heikkinen, R.K., Heinänen, S., Jones,
1183 A.R., Krishnakumar, P.K., Lauria, V., Lozano-Montes, H., Mannocci, L., Mellin, C., Mesgaran,
1184 M.B., Moreno-Amat, E., Mormede, S., Novaczek, E., Oppel, S., Ortuño Crespo, G., Peterson,
1185 A.T., Rapacciuolo, G., Roberts, J.J., Ross, R.E., Scales, K.L., Schoeman, D., Snelgrove, P.,
1186 Sundblad, G., Thuiller, W., Torres, L.G., Verbruggen, H., Wang, L., Wenger, S., Whittingham,

M.J., Zharikov, Y., Zurell, D., Sequeira, A.M.M., 2018. Outstanding Challenges in the Transferability of Ecological Models. Trends Ecol. Evol. 33, 790–802. https://doi.org/10.1016/j.tree.2018.08.001

Zemp, D.C., Schleussner, C.F., Barbosa, H.M.J., Hirota, M., Montade, V., Sampaio, G., Staal, A., Wang-Erlandsson, L., Rammig, A., 2017. Self-amplified Amazon forest loss due to vegetation-atmosphere feedbacks. Nat. Commun. 8. https://doi.org/10.1038/ncomms14681

Figures

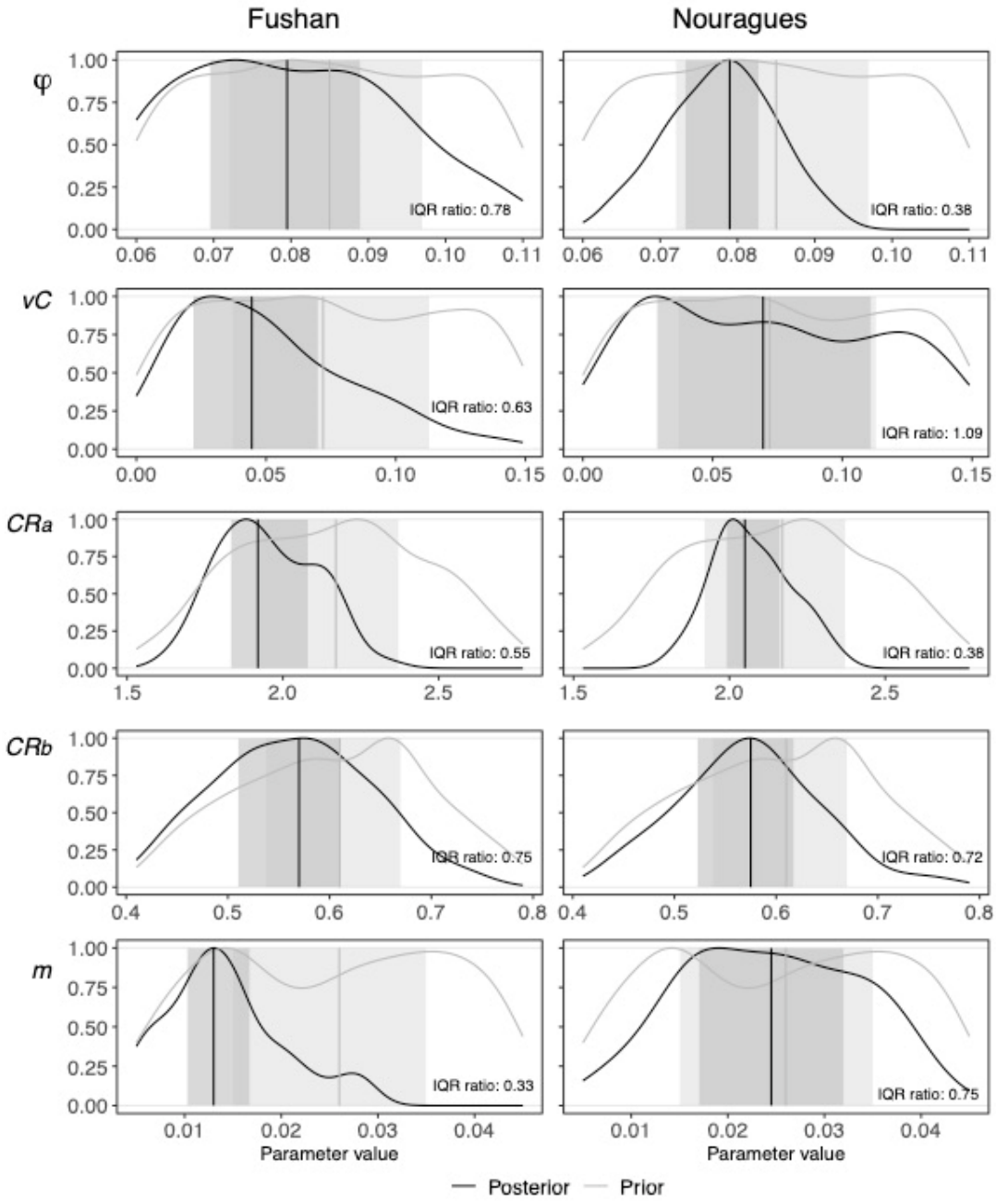

Figure 1. Prior (gray) and posterior (black) distributions for five parameters: φ (quantum yield), *vC* (treefall parameter), CR_a and CR_b (intercept and slope terms of the crown radius allometry), and *m* (background mortality). Results are reported for the Fushan site (Taiwan), and for the Nouragues site (French Guiana). Curves represent density functions, and vertical lines represent median value of the distributions. Shaded areas indicate interquartile range (IQR) of prior (light gray) and posterior (dark gray) distributions. IQR ratio is calculated as the posterior divided by prior IQR: lower IQR ratio is thus indicative of a higher parameter informativeness.

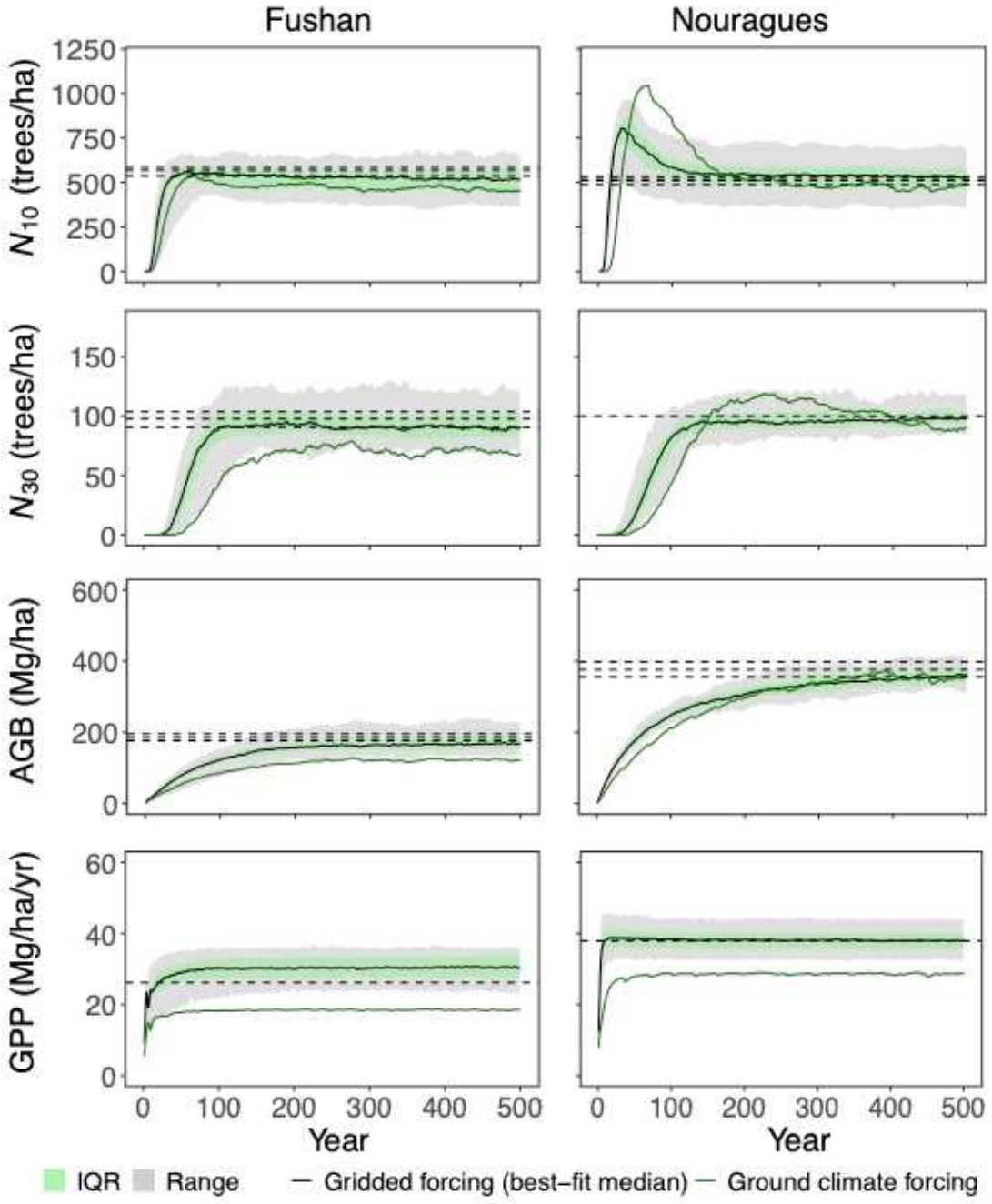

Figure 2. Successional dynamics of best-fit simulations at the Fushan and Nouragues sites, for four variables. Green shades represent the interquartile range, and gray shades represent the entire range of variation. Solid lines: median value of the best-fit simulations (black: gridded climate forcing; dark green: ground climate forcing); dashed lines: empirical values.

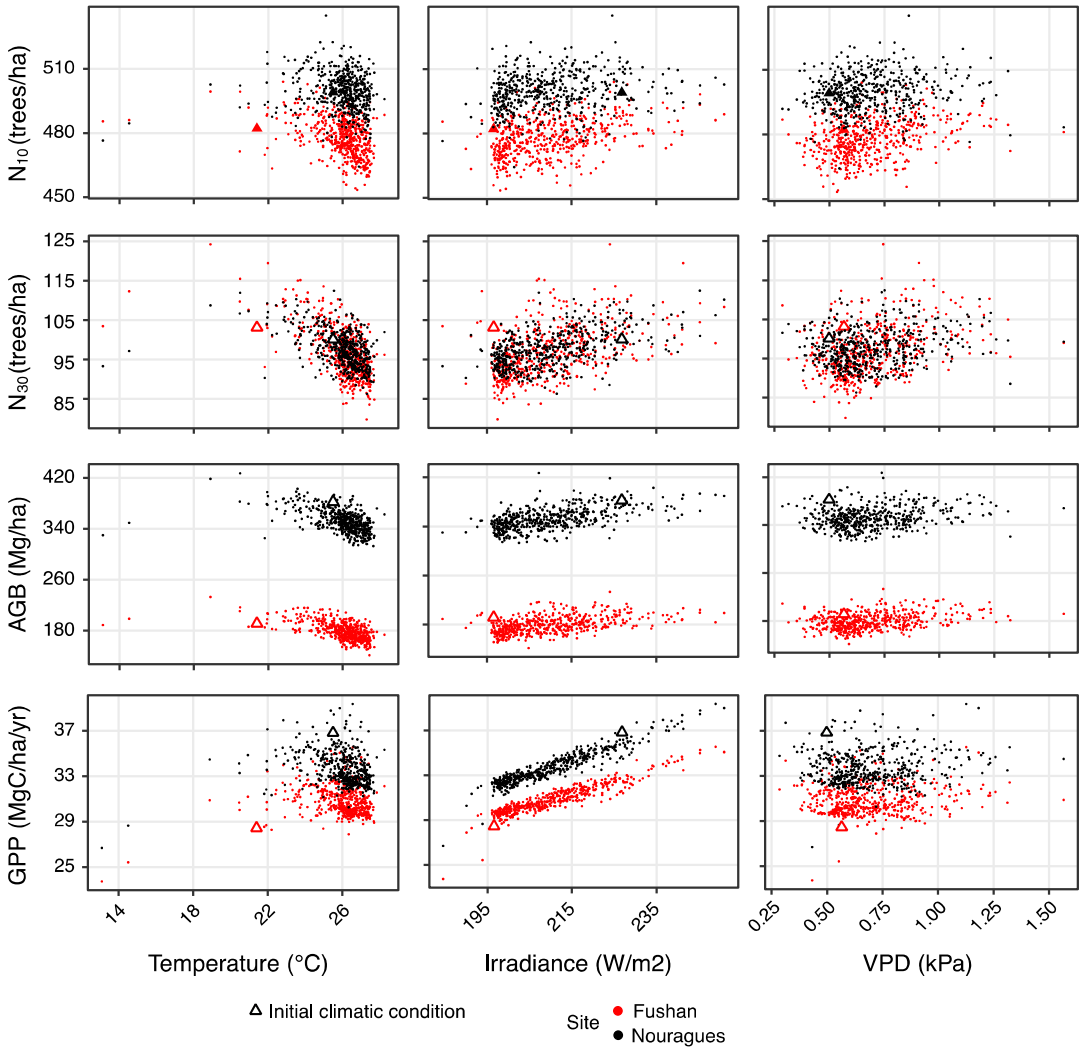

Figure 3. Effect of climatic conditions on forest structure and functioning at both sites (red: Fushan; black: Nouragues). Triangles indicate the simulations done under climatic condition of the original site.

Tables

	Description	Prior range
φ	quantum carbon yield per quantum photon	0.030-0.110 (Mercado *et al.* 2009)
vC	variability of the tree height-dependent stochastic treefall process	0.0-0.15
CR_a	intercept of the log-transformed CR-DBH allometry	1.5-2.8 (Fischer *et al.* 2020)
CR_b	slope of the log-transformed CR-DBH allometry	0.4-0.8 (Fischer *et al.* 2020)
m	maximal background mortality rate	0.005-0.045

Table 1. Parameters of the TROLL model calibrated at the two tropical forest sites.

Parameter	Fushan	Nouragues
φ	0.071 (0.070 – 0.089)	0.074 (0.073 – 0.082)
vC	0.099 (0.022 – 0.070)	0.031 (0.029 – 0.111)
CR_a	1.93 (1.833 – 2.080)	2.10 (1.990 – 2.163)
CR_b	0.51 (0.510 – 0.610)	0.57 (0.523 – 0.618)
m	0.006 (0.005 – 0.017)	0.023 (0.017 – 0.032)

Table 2. Optimal parameter values (parameter values of the simulation with best overall fit) at each site. Values in parentheses indicate the interquartile range of 50 best-fit simulations.

Metrics	Fushan	Nouragues
N_{10}	-14.4% (-18.1% – 0.8%)	-2.5% (-9.0% – 12.4%)
N_{30}	-5.9% (-14.9% – 5.3%)	0.1% (-8.4% – 4.2%)
AGB	-3.1% (-17.4% – 3.3%)	2.9% (-9.4% – 1.0%)
GPP	8.6% (5.6% – 28.5%)	-2.9% (-6.3% – 5.6%)

Table 3. Percentage difference between summary statistics of the optimal simulation (simulation with the best overall fit) and the mean empirical value. Values in parentheses indicate the interquartile range of percentage differences of the 50 best-fit simulations.

	Fushan				Nouragues			
	N_{10}	N_{30}	AGB	GPP	N_{10}	N_{30}	AGB	GPP
Temperature	**-0.341**	**-0.553**	**-0.489**	0.135	*-0.049*	**-0.385**	**-0.413**	0.032
Irradiance	0.251	0.296	**0.329**	**0.953**	0.142	**0.436**	**0.476**	**0.947**
VPD	0.228	0.230	0.183	-0.226	*0.061*	*0.039*	*0.027*	-0.202

Table 4. Effect size of each climatic variable on the output metrics at both sites, expressed in semi-partial correlation coefficients. Effect sizes with absolute values larger than 0.3 are indicated in bold. Italic indicates non-significant effects ($p > 0.05$).

Appendix A: generation of monthly mean climatic variables for TROLL input

Automated global reanalysis climate data calculation and extraction

The CRU-NCEP data are stored in NetCDF format, and the following variables are available: *Tair* for air temperature (K), *rain* for precipitation (mm), *WindN* and *WindE* for each of the two horizontal directional components of wind speed (m/s), SW*down* for incoming short-wave radiation exposure (J/m^2), *Qair* for air specific humidity, and *PSurf* for surface atmospheric pressure (Pa). We retrieved data for the period from 1980 to 2016, a period when many direct observations complemented model-based inferences in CRU-NCEP.

We processed the CRU-NCEP data across the entire land surface on Earth using the Climate Data Operators (cdo) tool (Schulzweida, 2019) and stored the results in NetCDF files, with a total of 74 files (2 files for each year). For each year, one file contains the monthly mean values of the following climatic variables: mean, maximum and minimum daily temperature (°C), mean and maximum daily irradiance (W/m^2), mean and maximum daily VPD (vapor pressure deficit, kPa), as well as monthly total precipitation (mm); another file contains the 6-hourly average wind speed (m/s), calculated as the quadratic average of the two wind speed components. Irradiance was calculated as the short-wave radiant exposure, divided by the time length of each measurement interval (6 hours, i.e. 6 × 3600 = 21600 seconds). VPD was calculated from temperature (T, °C), air specific humidity (R, unitless), and surface atmospheric pressure (P, kPa) with the following equations (Buck, 1981; Monteith and Unsworth, 2008):

$$VP_{sat} = 0.61121 \times e^{(18.678-\frac{T}{234.5})\times(\frac{T}{257.14+T})} \quad \text{(A1)}$$

$$VPD = VP_{sat} - \frac{R\times P}{0.622+0.378\times R} \quad \text{(A2)}$$

where VP_{sat} is the temperature-dependent saturated vapor pressure.

Subsequently, we used an R script to extract the monthly climatic variables from the files for a geographic coordinate, and generated a text file that is used as an input file for TROLL.

Appendix B: Data at Fushan FDP

At Fushan FDP, local meteorological data, daily from 1991 to 2012 and hourly from 2013 to 2016, was recorded at a meteorological station three kilometers east of Fushan FDP (24° 45′ N, 121° 35′ E). Temperature and humidity were measured by a Rotronic MP101A meteorological probe, precipitations by a tipping bucket rain gauge, irradiance by an E20 Silicon pyranometer (Homeray), and instantaneous wind speed by a Wind Monitor Model 05103 (Young).

In Fushan FDP, the sampling of functional traits was conducted in 2009, where 1 to 26 individuals per species were chosen randomly according to accessibility of tree canopy, and 1 to 3 intact and mature leaves or leaflets exposed to sunlight were collected for each individual. Collected leaves were sealed in Ziploc® bag with wet paper towels and kept in an insulated cooler box in order to prevent from water loss until transport back to the field station. There, the fresh weight of the leaves was measured to a precision of 0.1 mg, and they were scanned with a flatbed scanner within 12 hours. Leaf area (LA, cm^2) was quantified with the software ImageJ (Rasband 1997). The leaf samples were subsequently oven-dried at 80 °C for 72 - 96 hours, until constant dry weight. Leaf mass per area (LMA, g/m^2) were then calculated as dry weight divided by fresh leaf area (Pérez-Harguindeguy et al., 2013). Nitrogen and phosphorus content (N_{mass} and P_{mass}, mg/g) were determined by the microplate method (Huang et al., 2011; Iida et al., 2014).

Wood density (WD, g/cm^3) was measured following the ForestGEO wood density measurement protocol (Condit, 2008; Iida et al., 2014), by taking wood core samples of randomly chosen individuals outside the plot, measuring fresh volume by water displacement method and dry weight after oven-drying at 80 °C. Wood density was calculated as dry weight divided by fresh volume.

The allometric relationship between DBH and tree height (H) in the TROLL model was assumed to follow a Michaelis-Menten function with two parameters, asymptotic height (h_{max}) and the Michaelis constant (a_h), numerically equal to the diameter at which the tree height is half of h_{max}:

$$H = \frac{h_{max} \times DBH}{a_h + DBH} \quad \text{(B1)}$$

Although DBH values for all individuals were available, tree heights were only measured for 1 to 18 individuals for each species, depending on the accessibility of tree individuals. Due to the scarcity of available height data, a hierarchical Bayesian

model was used to estimate model parameters: the model assumed that the species-specific Michaelis-Menten parameters $h_{max,\,i}$ and $a_{h,\,i}$ for species i are distributed normally around common hyperparameters h_{max} and a_h (Molto et al., 2014). Parameters are close to the hyperparameters when data points are scarce for a particular species, while the species parameters dominate when data points are numerous for the species. Calculations were carried out with the software STAN and the R package *RStan* (Stan Development Team, 2016a, 2016b).

Appendix C: comparisons of different climate forcing sources.

The comparison between three climatic variables (temperature, precipitation, irradiance) extracted from CRU-NCEP data and ground station data showed that apart from minor differences, the climatic variables were largely congruent between CRU-NCEP and ground measures for the two ground study sites, the main difference being that seasonal variability for irradiance and precipitation was noticeably larger in ground data than in CRU-NCEP data at Fushan (Figure C1-2).

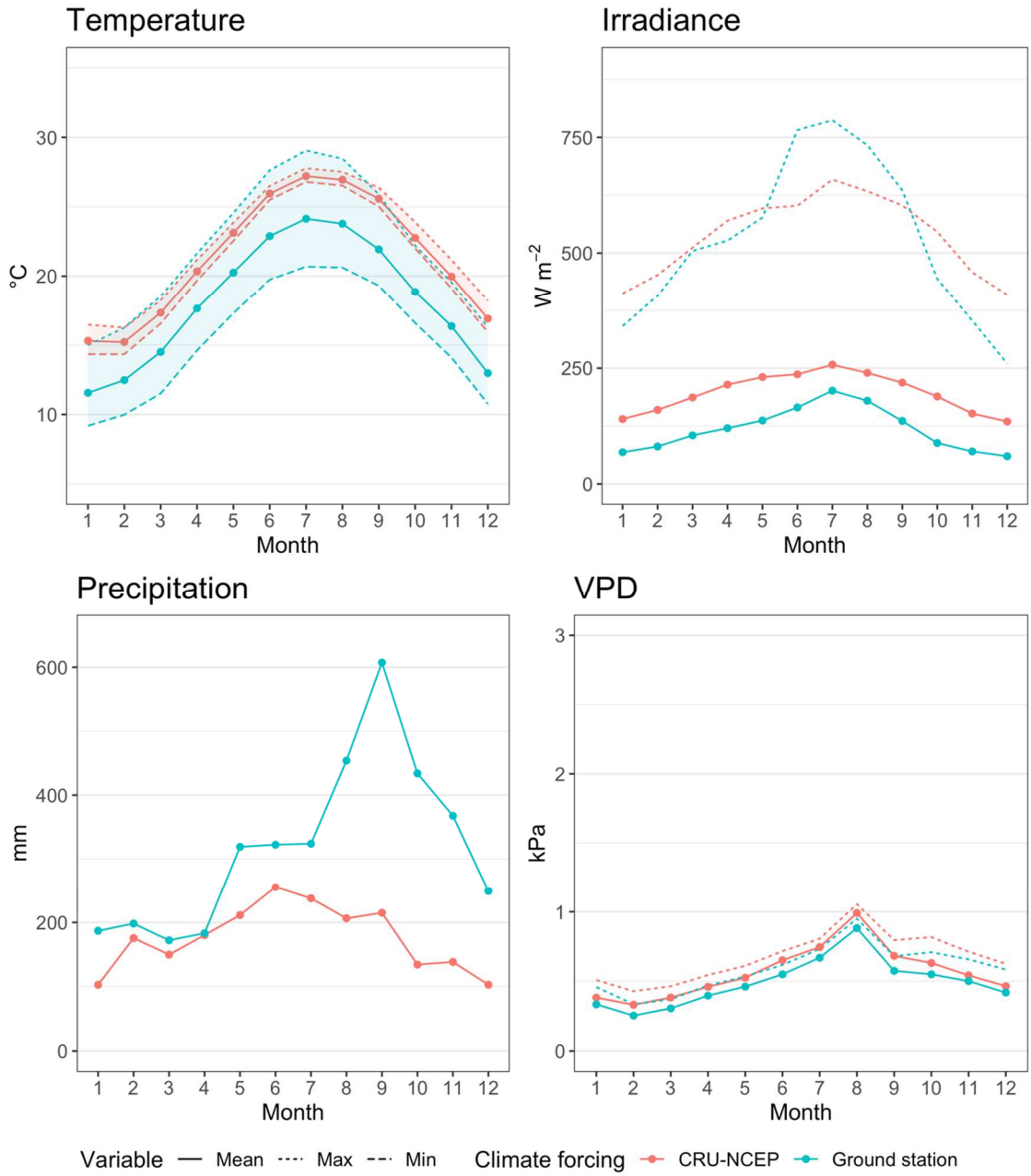

Figure C2. Comparison of climatic variables from CRU-NCEP gridded data or ground-based data at Nouragues.

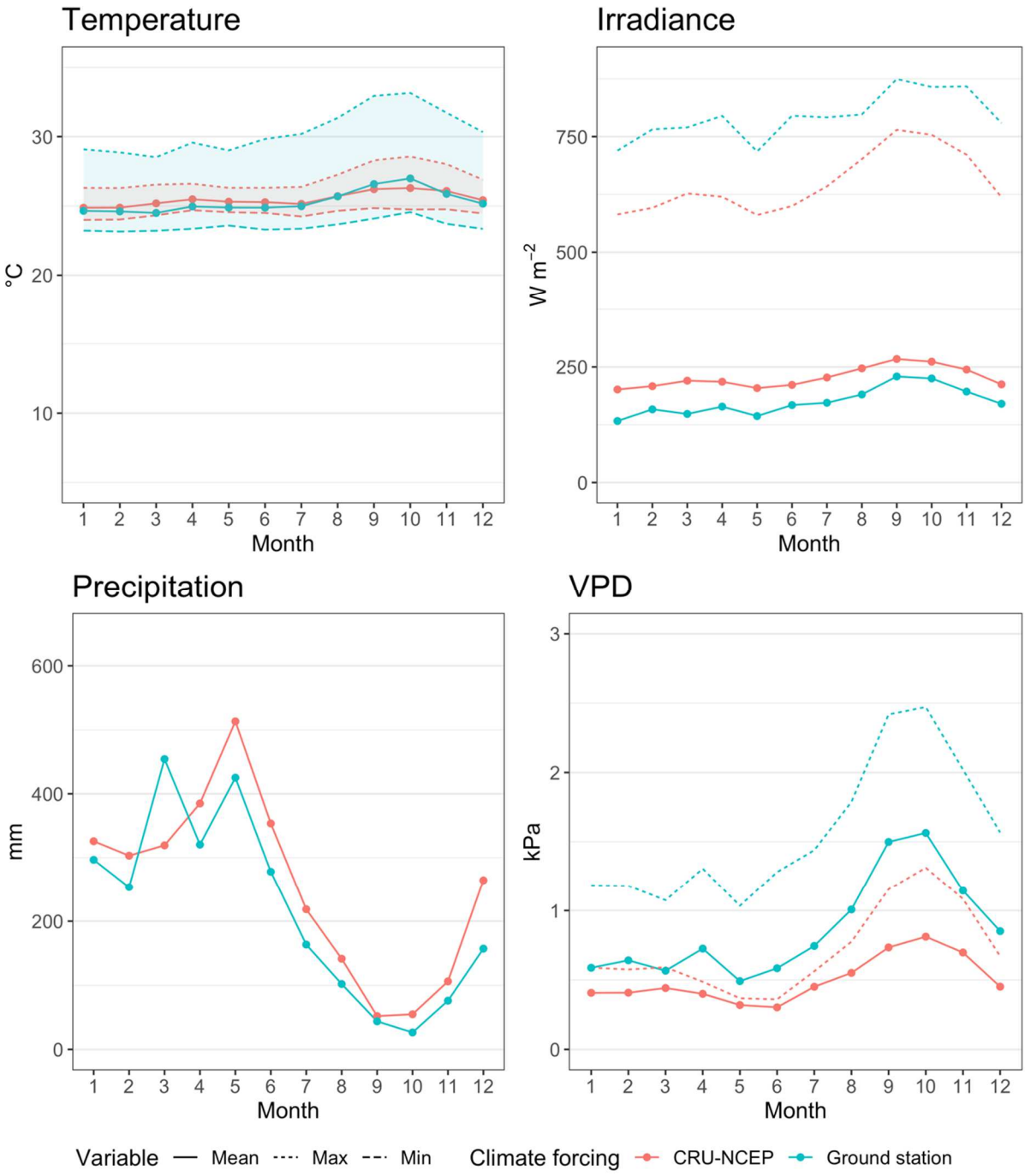

Figure C2. Comparison of climatic variables from CRU-NCEP gridded data or ground-based data at Nouragues.

Appendix D: preliminary parameter calibration

In the preliminary calibration tests, three other parameters were calibrated besides the parameters φ and *m*: *k*, the light extinction coefficient, describes the proportion of light extinction by each canopy layer; f_{wood} represents the fraction of assimilated carbon allocated to aboveground wood (branches and stem), and f_{canopy} represents the fraction allocated to canopy (twigs, leaves, and reproductive organs) (Table D1). We conducted the calibration tests following the same procedure as described in the main text, performing 500 simulations and selecting simulations with the 10% best overall fit (i.e., 50 simulations). The results indicated that model output was weakly sensitive to *k*; model sensitivity to f_{wood} and f_{canopy}, was non-negligible, but the overall model output did not deviate clearly from the observed value range no matter what their calibrated values were (Fig. D1 & D2). As a result, in all subsequent simulations we set a constant value for these three parameters. For *k*, we chose the lower bound value of 0.5 since reported values for forest ecosystems in Zhang *et al.* (2014) are primarily cluster around 0.5. For the allocation parameters, an intermediate value within the reported range was chosen (f_{wood} = 0.35, f_{canopy} = 0.25).

k	light extinction coefficient	0.50-0.95 (Cournac *et al.* 2002, Zhang *et al.* 2014)
φ	quantum carbon yield per quantum photon	0.030-0.110 (Mercado *et al.* 2009)
f_{wood}	fraction of NPP allocated to aboveground wood	0.20-0.45 (Aragão *et al.* 2009, Malhi *et al.* 2011)
f_{canopy}	fraction of NPP allocated to canopy	0.20-0.45 (Aragão *et al.* 2009, Malhi *et al.* 2011)
m	maximal background mortality rate	0.005-0.045

Table D1. Parameters of the TROLL model calibrated at the two tropical forest sites in preliminary tests.

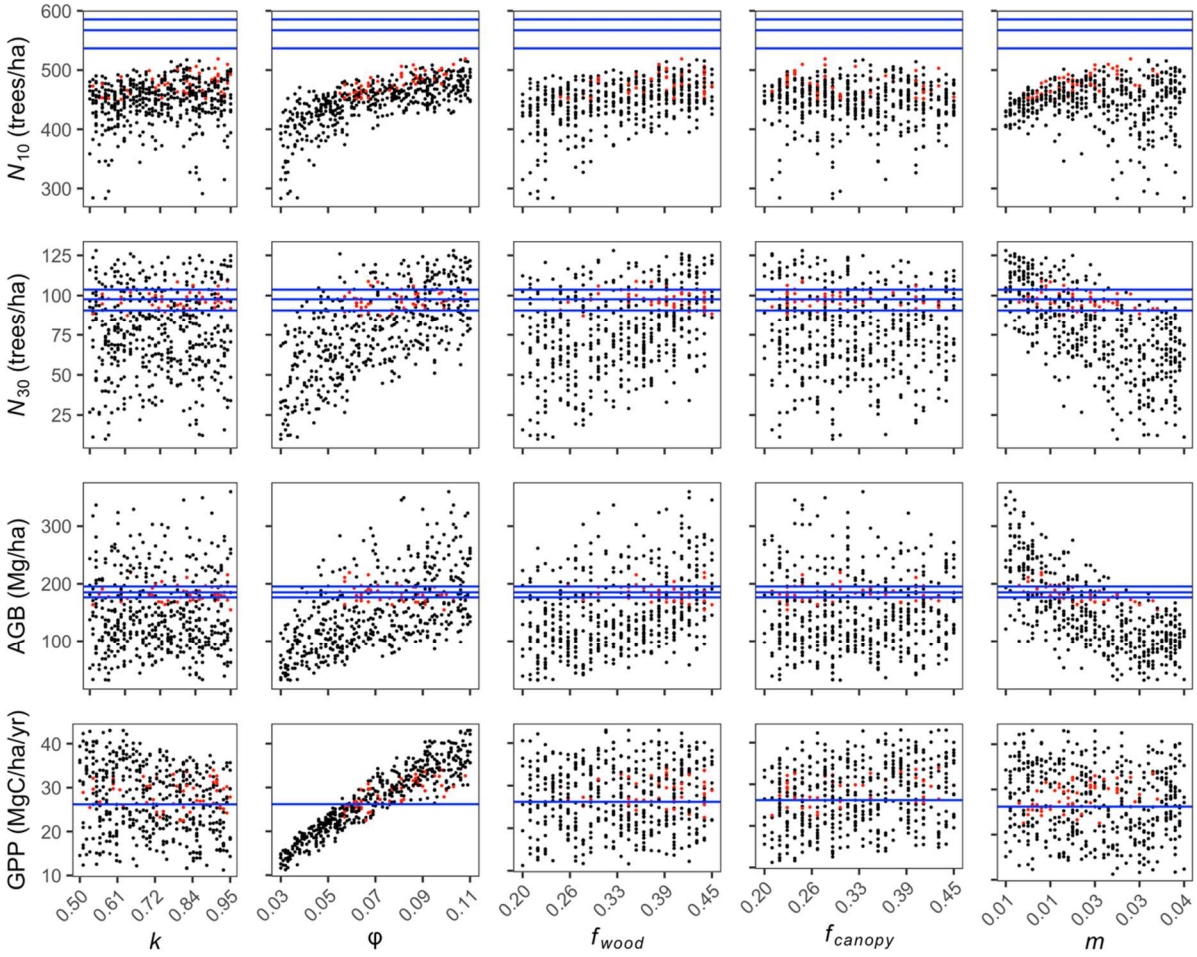

Figure D1. Calibration of TROLL general parameters for Fushan (*k*: light extinction coefficient; φ: quantum yield; f_{wood} and f_{canopy}: carbon allocation to different plant organs; *m*: background mortality). Horizontal blue lines are observed values from field censuses. Each point represents one simulation, and red points are best-fit simulations.

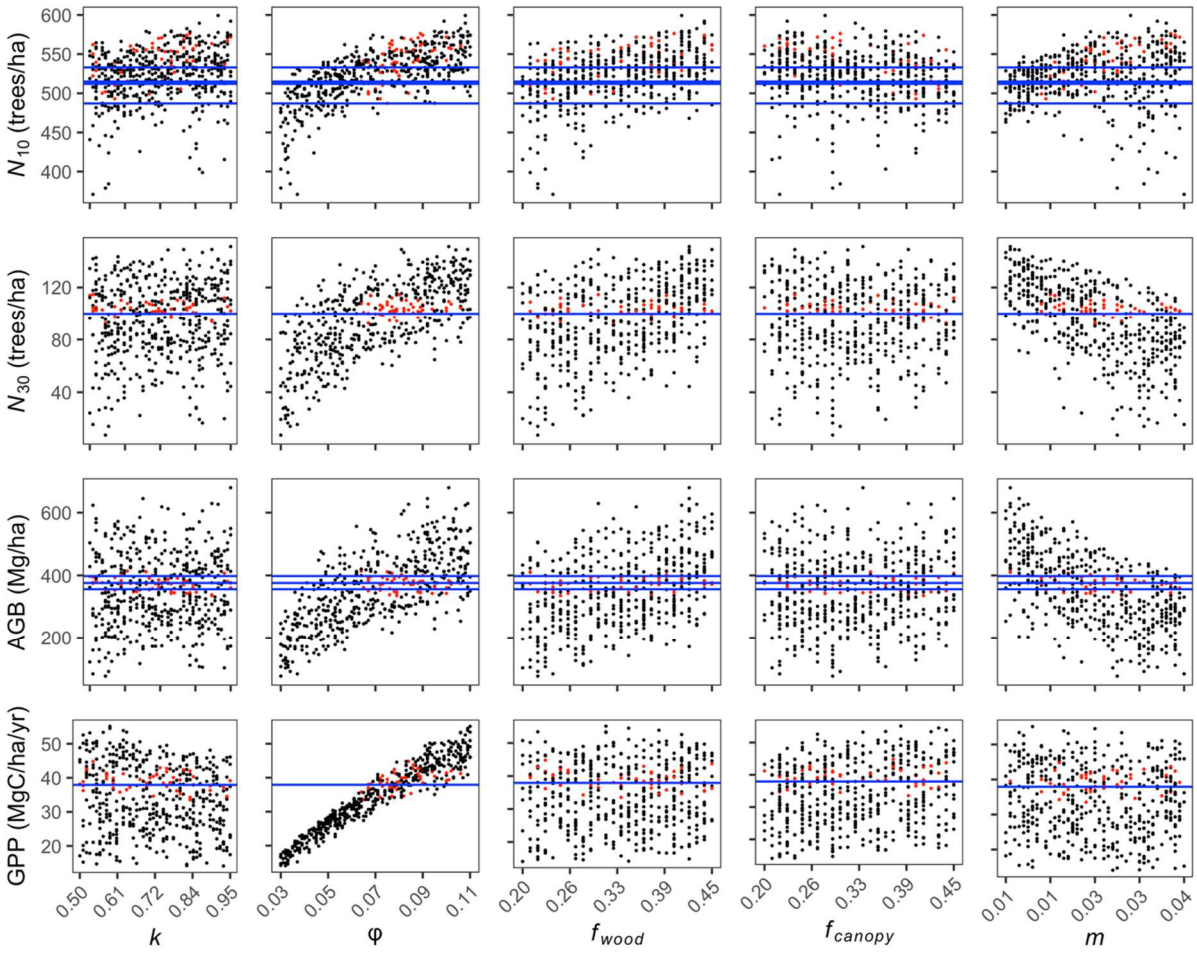

Figure D2. Calibration of TROLL general parameters for Nouragues (*k*: light extinction coefficient; φ: quantum yield; f_{wood} and f_{canopy}: carbon allocation to different plant organs; *m*: background mortality). Horizontal blue lines are observed values from field censuses. Each point represents one simulation, and red points are best-fit simulations.

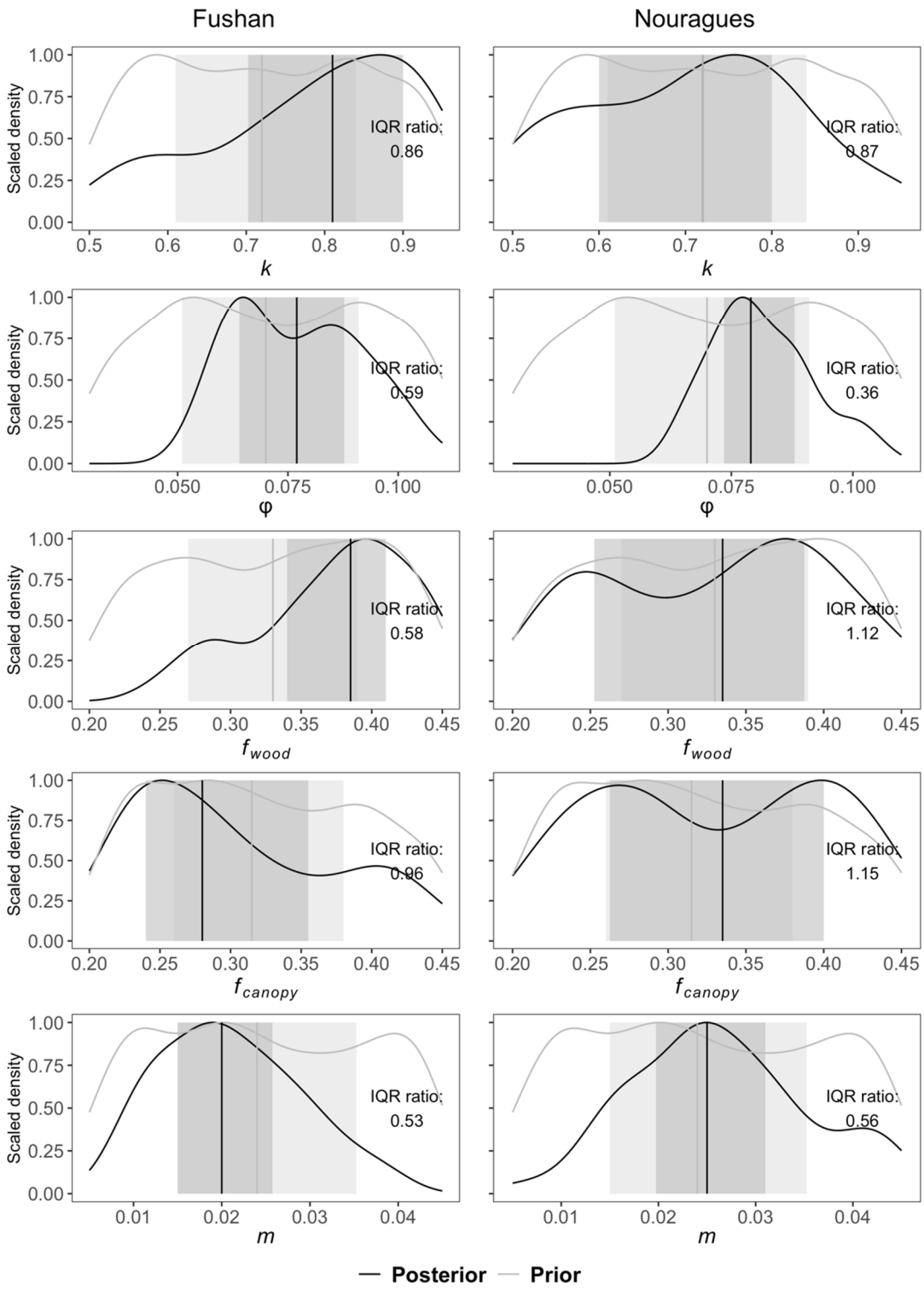

Figure D3. Prior (grey) and posterior (black) density distributions for parameter values (*k*: light extinction coefficient; φ: quantum yield; f_{wood} and f_{canopy}: carbon allocation to different plant organs; *m*: background mortality). Solid vertical lines indicate median and dashed vertical lines indicate interquartile range (IQR). Parameter informativeness is calculated as the ratio between IQR of best-fit simulations and that of all simulations.

Appendix E: parameter calibration

We conducted calibration tests on five parameters: φ (quantum carbon yield per quantum photon), *vC* (variability of the tree height-dependent stochastic treefall process) CR_a, CR_b (intercept and slope terms of the log-transformed CR-DBH allometry), and *m* (maximal background mortality rate), following the procedure as described in the main text, performing 500 simulations and selecting simulations with the 10% best overall fit (i.e., 50 simulations). The results showed that model output was strongly sensitive to φ, CR_a and *m*, and to a lesser exten to CR_b.

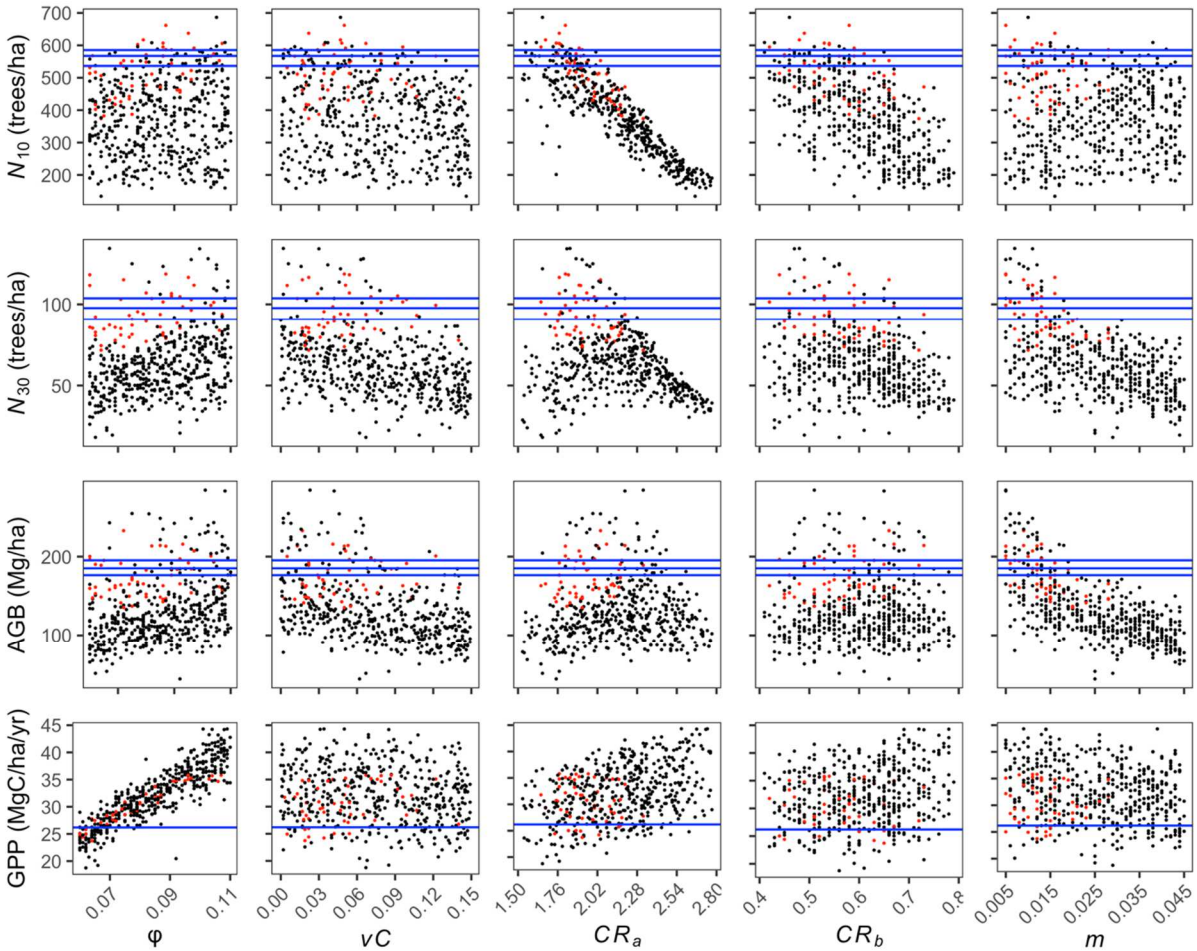

Figure E1. Calibration of TROLL general parameters (φ: quantum yield; *vC*: treefall parameter; CR_a and CR_b: intercept and slope terms of the crown radius allometry; *m*: background mortality) for Fushan. Horizontal blue lines are observed values from field censuses. Each point represents one simulation, and red points are the best-fit simulations (10% best simulations).

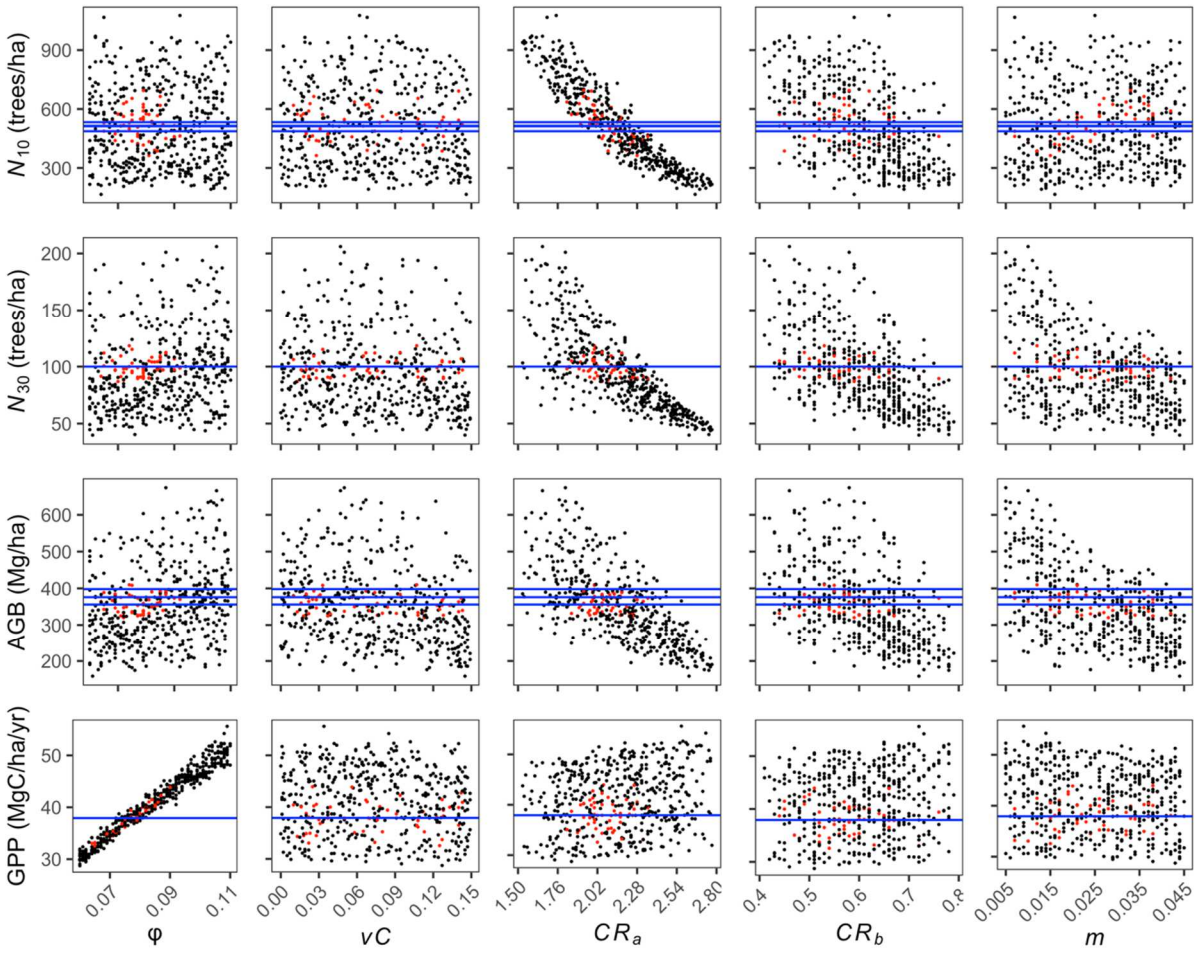

Figure E2. Calibration of TROLL general parameters (φ: quantum yield; *vC*: treefall parameter; CR_a and CR_b: intercept and slope terms of the crown radius allometry; *m*: background mortality) for Nouragues. Horizontal blue lines are observed values from field censuses. Each point represents one simulation, and red points are the best-fit simulations (10% best simulations).

Appendix F: verification of assumptions for linear model for the sampled climate experiment

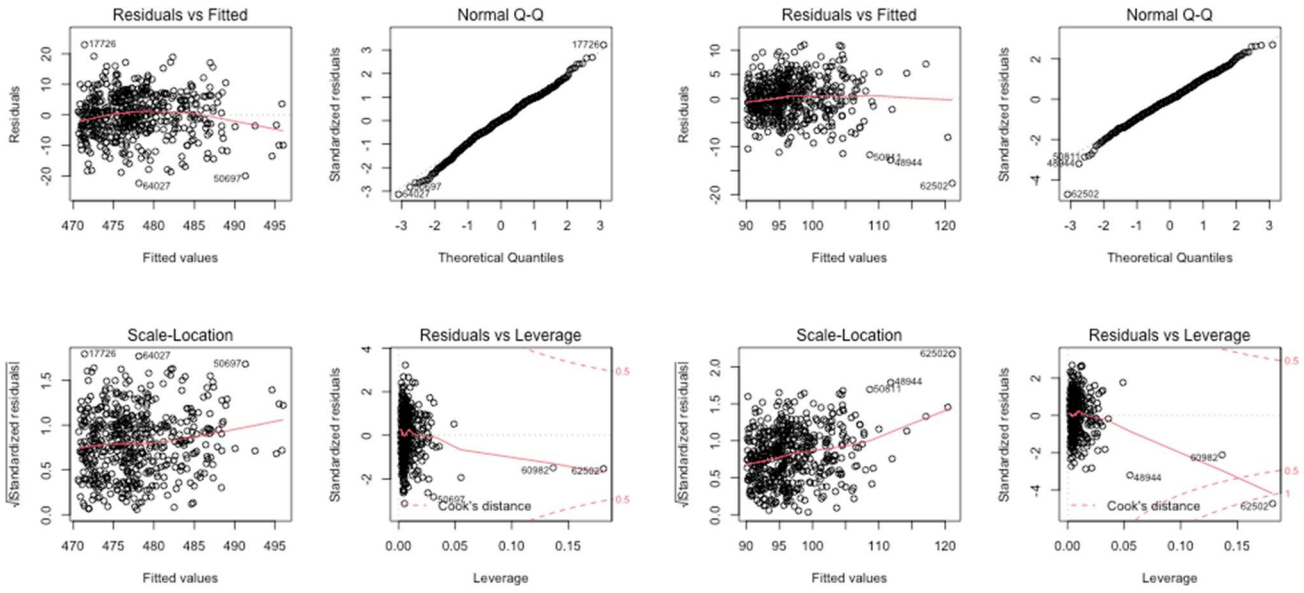

N10 N30

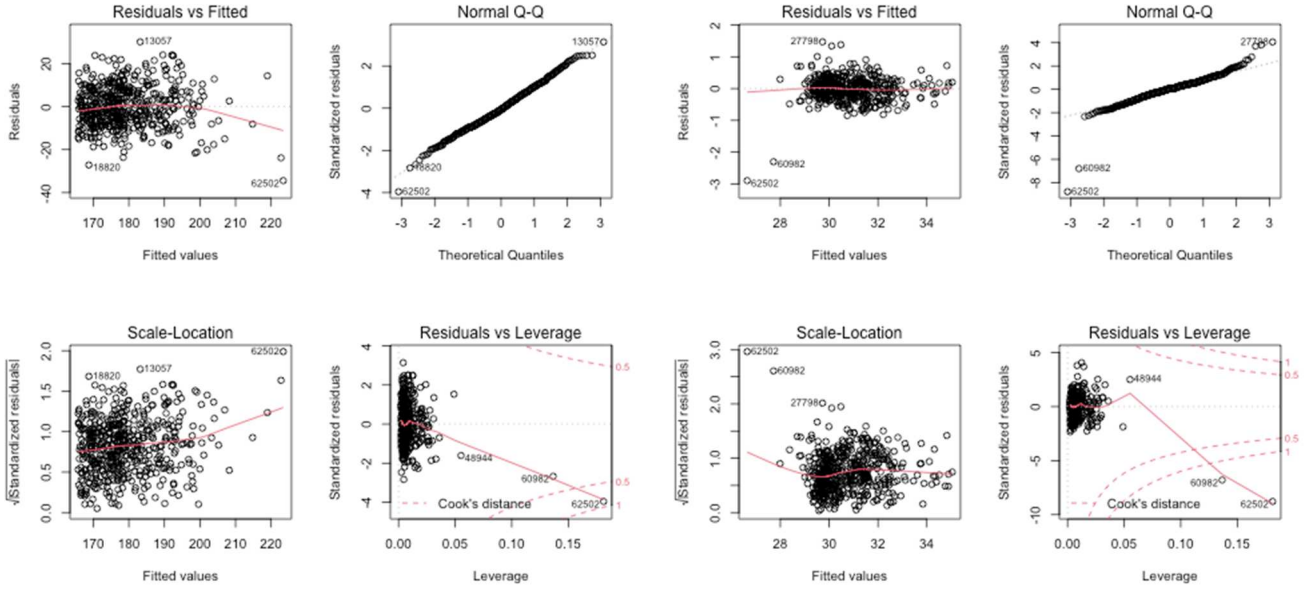

AGB GPP

Figure F1. Diagnostic plots of linear model for the sampled climate experiment at Fushan, with each summary statistics as dependent variables and the three climatic variables (temperature, irradiance and VPD) as independent variables. The four graphs represent respectively residual linearity, residual normality, residual homoscedasticity, and presence or absence of leverage points (influential points).

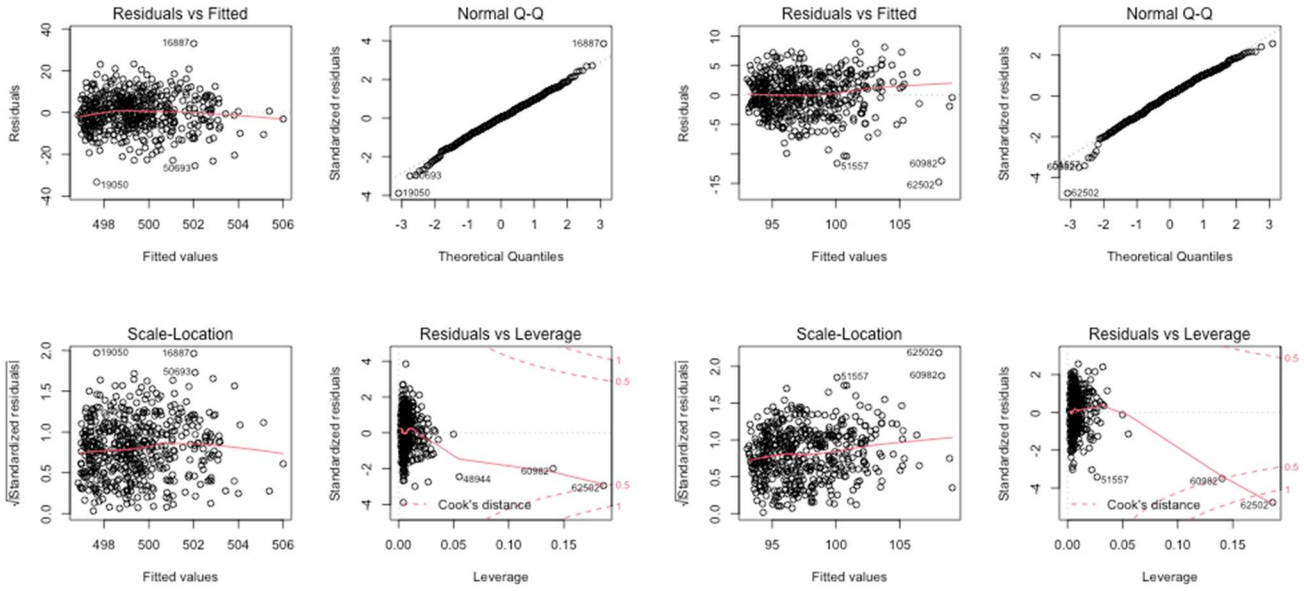

N10 N30

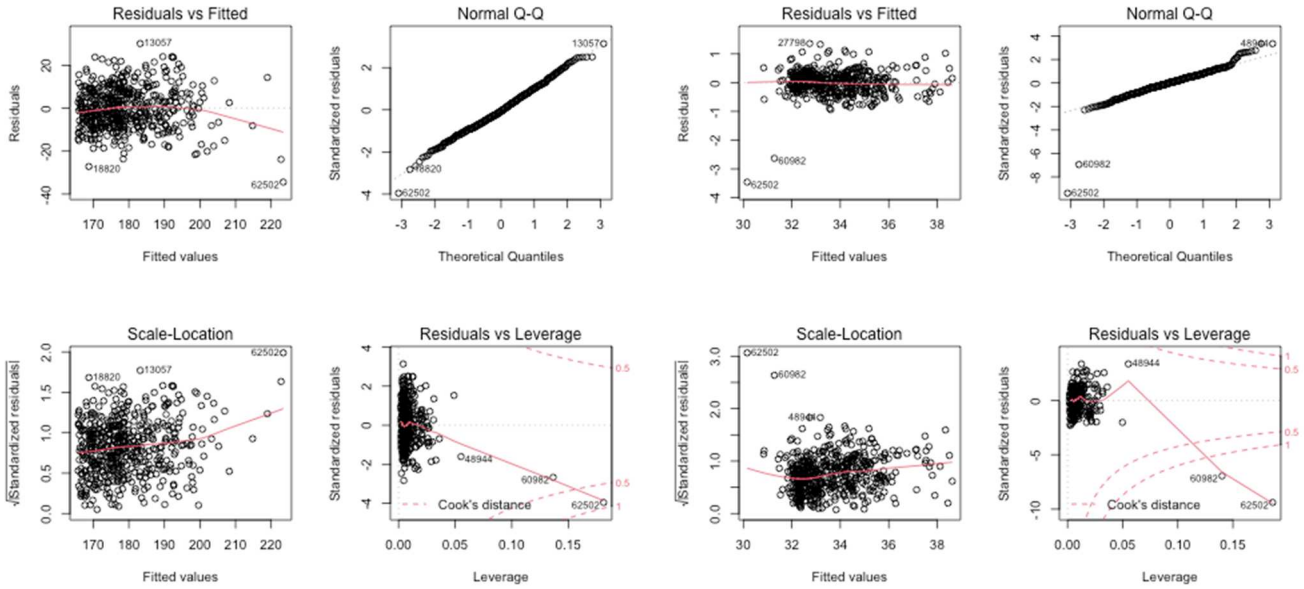

AGB GPP

Figure F2. Diagnostic plots of linear model for the sampled climate experiment at Nouragues, with each summary statistics as dependent variables and the three climatic variables (temperature, irradiance and VPD) as independent variables. The four graphs represent, respectively, residual linearity, residual normality, residual homoscedasticity, and presence or absence of leverage points (influential points).

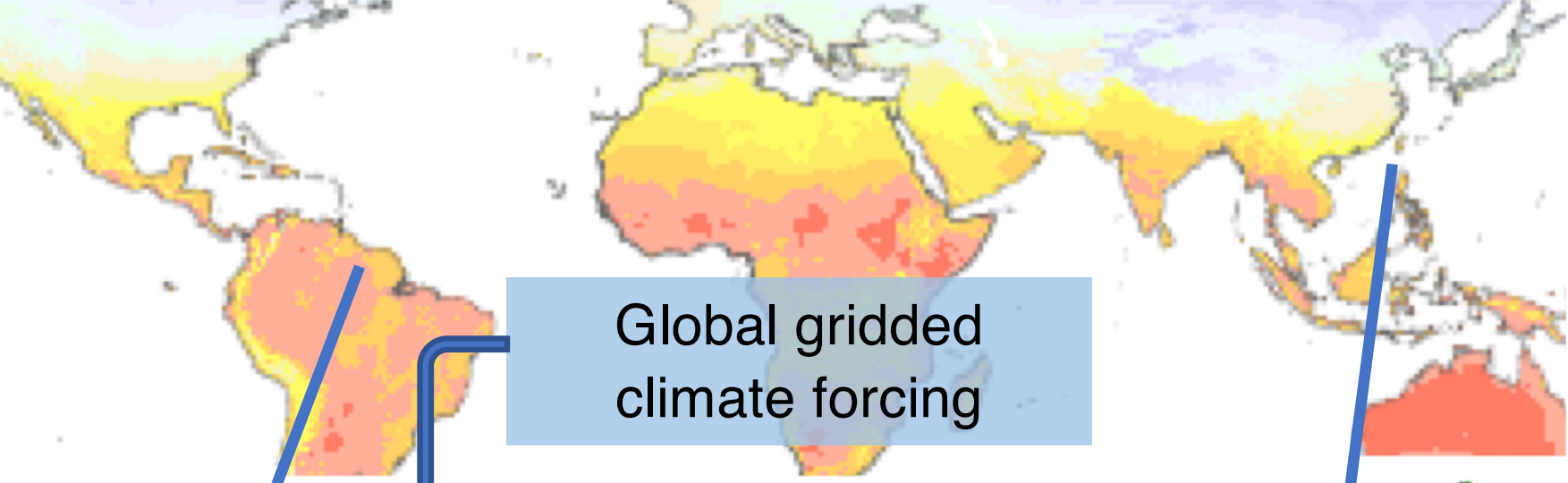

Global gridded climate forcing

Local data sets
Climate
Plant functional traits

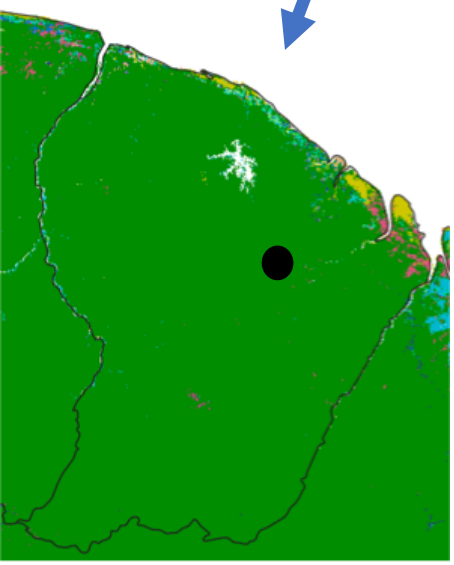

French Guiana

Parameter calibration

Taiwan

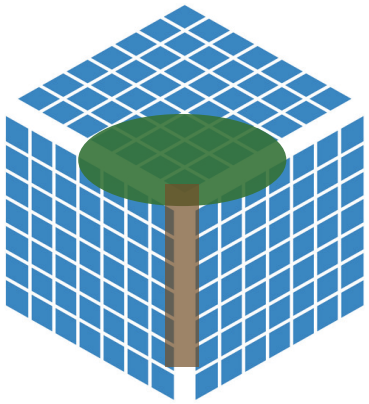

Individual-based forest growth model

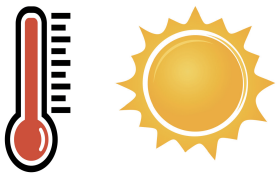

Climate experiment